Density functional calculations on graphene structures with WIEN2k

Bachelor thesis

Summer term 2014

University of Regensburg

Faculty of Physics

Author:

Klaus Zollner

Matriculation number:

156 022 9

Supervisors:

Prof. Dr. Jaroslav Fabian

Tobias Frank

July 2014

Contents

1 Introduction

The big interest in condensed matter physics is due to the possibility to find new materials, that allow to improve the performance of for example electrical devices, such as transistors and build these at nanoscale size. Another branch of research in this area is spintronics, where one hopes to gain control over the spin degree of freedom, in special materials, to obtain new possibilities in information processing (supercomputer). A very promising and highly discussed material in condensed matter physics is graphene.
Graphene is a very special solid with some unique properties. Because of its hexagonal single layer structure it is light as well as robust and flexible. In recent years it has always been a great subject in research with a lot of applications. For instance it is used in integrated circuits (high charge carrier mobility), in solar cells (high electric conductivity and optical transparency) or in so called graphene-based ultracapacitors (energy storage). Moreover it is claimed to be the ideal material for spintronics [20].

This work handles with the problem how to calculate some of these properties (electronic density, band structure) with the density functional theory (DFT) on the basis of the WIEN2k code [10].
Some theoretical background is needed to understand the major problem, because it is very difficult to handle a many particle system. Therefore a short introduction on solid state physics is given, where the many-particle Hamiltonian gets constructed. The next step is to find good approaches, to simplify the problem, but not neglect too much important contributions. The Born-Oppenheimer approximation is therefore introduced, which neglects the motion of the nuclei, because of their much bigger mass than those of the electrons.
The important element in DFT is the electronic density, which contains equivalent information

as the many body wave function, according to the theorems of Hohenberg and Kohn [8]. Out of these follow the Kohn-Sham equations [9], which is a self consistency problem, that can be solved, when making further approximation for the exchange-correlation potential (LDA, GGA). The accuracy of the final solution depends on the used basis set and its size (APW, LAPW, APW+lo).
In the last part the WIEN2k code and its operating principle is shortly introduced and the results on the single layer graphene calculations are presented. The more important and interesting part is the one, where we consider methylated graphene. This is a single graphene layer, where methyl groups (CH_3 molecules) are attached, so that one might find interesting new properties, which could be useful and applicable in technology.

2 Many-particle systems

In solid-state physics one has to deal with properties of matter in the solid phase. A solid is composed of atoms, that are held together by chemical bonding. The number of atoms is typically $N \sim 10^{23}$ and hence properties of solids have to be investigated using methods of quantum mechanics combined with those of statistical physics. The difficulty comes from the fact that the constituents in a solid (nuclei, electrons) interact among themselves through Coulomb interaction.

2.1 Many-body-Hamiltonian

To describe the microscopic properties of a solid, one first needs to know the Hamiltonian of this system. The kinetic energy divides into the one for the electrons and the one for the nuclei. Considering only the relevant scales for a solid, the only interaction is the Coulomb-interaction, between all of the different constituents. The Hamiltonian then reads [1]

$$\hat{H} = \hat{T}_e + \hat{T}_n + \hat{V}_{ee} + \hat{V}_{nn} + \hat{V}_{en}. \tag{2.1}$$

The single parts of the Hamiltonian in their explicit forms are:

- the kinetic energy of the electrons

$$\hat{T}_e = -\sum_i \frac{\hbar^2}{2m_e} \nabla_i^2 \tag{2.2}$$

- the kinetic energy of the nuclei

$$\hat{T}_n = -\sum_I \frac{\hbar^2}{2M_I} \nabla_I^2 \tag{2.3}$$

- the potential energy from the Coulomb interaction between the electrons

$$\hat{V}_{ee} = \frac{1}{2} \sum_{i \neq j} \frac{e^2}{|\boldsymbol{r}_i - \boldsymbol{r}_j|} \tag{2.4}$$

- the potential energy from the Coulomb interaction between the nuclei

$$\hat{V}_{nn} = \frac{1}{2} \sum_{I \neq J} \frac{Z_I Z_J e^2}{|\boldsymbol{R}_I - \boldsymbol{R}_J|} \tag{2.5}$$

- the potential energy from the Coulomb interaction between the electrons and the nuclei

$$\hat{V}_{en} = -\sum_{i,I} \frac{Z_I e^2}{|\boldsymbol{r}_i - \boldsymbol{R}_I|} \tag{2.6}$$

As one can already see now, the Hamiltonian contains a lot of terms, because of the huge number of interacting particles. Therefore the problem is to develop methods to handle this with an accuracy, so that nothing important is neglected.

2.2 Many-body Schrödinger equation and wave function

The Hamiltonian 2.1 can describe all kinds of materials (plastic, glass, steel, ...), because it is general and exact for all solids. The Schrödinger equation for the given problem is

$$\hat{H}\Psi = E\Psi, \tag{2.7}$$

where

$$\Psi = \Psi(\{\boldsymbol{r}_i\}, \{\boldsymbol{R}_I\}), \tag{2.8}$$

depends on all coordinates of the electrons $\{\boldsymbol{r}_i\}$ and the coordinates of the nuclei $\{\boldsymbol{R}_I\}$. The main issue is, that already a problem of three particles is not solvable, when interactions play a role. For simplifications, we do not consider the spin here, but it could be easily added in the formalism. So we are looking at a system of N indistinguishable particles. As we only consider electrons in the main part (after chapter 2.3 this will be clear), the wave function has the form

$$\Psi = \Psi(1, 2, \ldots, N). \tag{2.9}$$

Introducing the permutation operator $\hat{P}_{ij}$, which interchanges two particles at i and j

$$\hat{P}_{ij}\Psi(1, 2, \ldots, i, j, \ldots, N) = \Psi(1, 2, \ldots, j, i, \ldots, N), \tag{2.10}$$

leads to

$$\hat{P}_{ij}\Psi = -\Psi, \tag{2.11}$$

as electrons are fermions and the wave function must be antisymmetric. One can also show, that if Ψ is an eigenstate, $\hat{P}\Psi$ also is, where $\hat{P}$ is a general permutation. Therefore any

observable $\hat{A}$, especially $\hat{H}$, commutes with $\hat{P}$

$$[\hat{P}, \hat{A}] = 0 \quad \Rightarrow \quad \langle \hat{P}\Psi | \hat{A} | \hat{P}\Psi \rangle = \langle \Psi | \hat{A} | \Psi \rangle. \tag{2.12}$$

$\hat{P}$ is unitary, which means $\hat{P}^\dagger = \hat{P}^{-1}$. In general the antisymmetric N-particle wave function is

$$\Psi_A(\{\boldsymbol{r}_i\}) = \frac{1}{\sqrt{N!}} \begin{vmatrix} \phi_{\alpha_1}(\boldsymbol{r}_1) & \cdots & \phi_{\alpha_1}(\boldsymbol{r}_N) \\ \vdots & & \vdots \\ \phi_{\alpha_N}(\boldsymbol{r}_1) & \cdots & \phi_{\alpha_N}(\boldsymbol{r}_N) \end{vmatrix}, \tag{2.13}$$

with the single particle states $\phi_{\alpha_i}(\boldsymbol{r}_j)$. This is the Slater-determinant representation, which has the required properties of antisymmetry (interchanging columns gives a *-1*) and satisfies the Pauli-principle ($\alpha_i = \alpha_j \;\Rightarrow\; \Psi_A = 0$), where no state can be double occupied.

2.3 Born-Oppenheimer approximation

On closer examination of the Hamiltonian 2.1 with the explicit form of the single parts one notices that there is a *small* term contained in comparison to others. Looking at the masses of the constituents one finds $\frac{m_e}{M_I} \sim 10^{-4}$ and therefore the kinetic energy of the nuclei is much smaller than the one of the electrons. Electrons adopt instantaneously to the actual configuration of the nuclei. One can get a qualitative proof of this by assuming the whole system to be in thermal equilibrium. Electrons and Nuclei have the same thermal energy per degree of freedom

$$\left\langle \frac{m_e}{2} v_i^2 \right\rangle = \left\langle \frac{M_I}{2} v_I^2 \right\rangle = \frac{k_B T}{2}. \tag{2.14}$$

Due to $\frac{m_e}{M_I} \sim 10^{-4}$, electrons move much faster. This leads to the fact, that one can consider the electrons to be in a system, with a positive charge distribution, from the fixed nuclei. Therefore, electrons are the only particles we now need to describe with our wave function. The consequences of the Born-Oppenheimer approximation [5] are, that the exact Hamiltonian 2.1 reduces to

$$\hat{H} = \hat{T}_e + \hat{V}_{ee} + \hat{V}_{ext} + E_1. \tag{2.15}$$

Because of the fixed position of the nuclei, their kinetic energy is zero. The interaction term between the nuclei reduces to a constant E_1, which just leads to an energy shift and is irrelevant when calculating the electronic wave function. The actual effect of the nuclei on the electrons is now contained in the *external* potential $\hat{V}_{ext}$. A more general form for the external potential would now be

$$\hat{V}_{ext} = \sum_{i,I} V_I(|\boldsymbol{r}_i - \boldsymbol{R}_I|), \tag{2.16}$$

which contains the Coulomb interaction, but can also include additional terms like an electric field [1]. However the central Hamiltonian we now have to deal with is

$$\hat{H} = \hat{T}_e + \hat{V}_{ee} + \hat{V}_{ext} = \hat{H}_{el} + \hat{V}_{ext}, \tag{2.17}$$

with a system-independent part $\hat{H}_{el}$ and a part $\hat{V}_{ext}$ which contains all the system-relevant information. Therefore we now have a wave function $\Psi(\{\boldsymbol{r}_i\})$, which only depends on the coordinates $\boldsymbol{r}_i$ of the electrons, since the position of the nuclei is fixed. Note, that there also exists an effective Schrödinger equation for the nuclei, where the energy of the electrons acts like an effective potential, but this is not important, since we want to describe electronic properties.

3 Density functional theory

Despite the Born-Oppenheimer approximation, the given Hamiltonian is still too difficult. Therefore one wants to work with a simpler approximation picture, because the problem is not exactly solvable. A lot of solution methods exist in order to deal with the quantum many-body problem, given through the Hamiltonian 2.17. A commonly used method is the Hartree-Fock approximation because it works very well for atoms and molecules. For solids, this method is not so accurate and therefore a more modern one is used, namely *Density Functional Theory* (DFT). This method was established by P. Hohenberg and W. Kohn (HK) in 1964. The most important quantity in this formalism is the electronic density $\rho(\boldsymbol{r})$

$$\rho(\boldsymbol{r}) = \sum_{i=1}^{N} |\phi_i(\boldsymbol{r})|^2, \tag{3.1}$$

contrary to the formalism of Schrödinger, where the wave function $\Psi(\boldsymbol{r}_i)$ plays the central role. At first sight, one thinks, that the density, which only depends on three parameters $\boldsymbol{r}$, cannot provide the same information as the wave function, which depends on $3N$ parameters $\boldsymbol{r}_i$, but the theorems of HK [8] prove the opposite.

3.1 Hohenberg-Kohn theorems

Theorem 1: The ground state density $\rho(\boldsymbol{r})$ defines uniquely the Hamiltonian. Therefore the many particle ground state energy is a unique functional of the density $\rho(\boldsymbol{r})$ [8].

Proof: Suppose the same density $\rho(\boldsymbol{r})$ follows from two different external potentials $\hat{V}_{ext}$ and $\hat{V}'_{ext}$ (they should differ not only by a constant) and therefore two different Hamiltonians $\hat{H}$ and $\hat{H}'$. The wave functions Ψ and Ψ' are not equal, because they are the solutions to different Schrödinger equations.

$$\hat{H} = \hat{H}_{el} + \hat{V}_{ext} \neq \hat{H}_{el} + \hat{V}'_{ext} = \hat{H}' \tag{3.2}$$

$$\hat{H}\Psi = E_0\Psi, \qquad \hat{H}'\Psi' = E'_0\Psi', \qquad E_0 \neq E'_0 \tag{3.3}$$

Using the minimal principle one can say

$$E_0 = \langle\Psi|\hat{H}|\Psi\rangle < \langle\Psi'|\hat{H}|\Psi'\rangle = \langle\Psi'|\hat{H}'|\Psi'\rangle + \langle\Psi'|\hat{H} - \hat{H}'|\Psi'\rangle, \tag{3.4}$$

$$E_0 < E_0' + \int d^3r\rho(\boldsymbol{r})(\hat{V}_{ext} - \hat{V}_{ext}'), \tag{3.5}$$

The same can be done, when interchanging primed and unprimed quantities

$$E_0' < E_0 - \int d^3r\rho(\boldsymbol{r})(\hat{V}_{ext} - \hat{V}_{ext}'), \tag{3.6}$$

which leads to contradiction, when adding equations 3.5 and 3.6 . This proves, that the ground state energy is a unique functional of the density.

Theorem 2: For the Hamiltonian $\hat{H}$, the ground state energy functional is defined by

$$H[\rho] = E_{V_{ext}}[\rho] = \langle\Psi|\hat{H}_{el} + \hat{V}_{ext}|\Psi\rangle = F_{HK}[\rho] + \int \rho(\boldsymbol{r})\hat{V}_{ext}(\boldsymbol{r})d\boldsymbol{r}, \tag{3.7}$$

and reaches its minimal value for the ground state density $\rho(\boldsymbol{r})$, corresponding to $\hat{H}$ [8].

Proof: The energy functional for a system of N particles depending on Ψ' is given by

$$E[\Psi'] = \langle\Psi'|\hat{H}|\Psi'\rangle, \tag{3.8}$$

and has its minimum at the correct ground state Ψ, under the constraint that the particle number is constant

$$N[\rho] = \int \rho(\boldsymbol{r})d\boldsymbol{r} = N. \tag{3.9}$$

Using equation 3.7 leads to

$$E[\Psi'] = F_{HK}[\rho'] + \int \rho'(\boldsymbol{r})\hat{V}_{ext}(\boldsymbol{r})d\boldsymbol{r} \;>\; F_{HK}[\rho] + \int \rho(\boldsymbol{r})\hat{V}_{ext}(\boldsymbol{r})d\boldsymbol{r} = E[\Psi], \tag{3.10}$$

which proves, that $E_{V_{ext}}[\rho]$ reaches its minimal value for the ground state density.
A definitely advantage of these theorems is, that we now have to search for the correct ground state density, which depends only on three parameters. Because of the fact that the Coulomb interaction has a rather long range, one can separate the classical Coulomb energy. Hence for most purposes it is appropriate to rewrite $F_{HK}[\rho]$ in the following way

$$F_{HK}[\rho] = \frac{1}{2}\int \frac{\rho(\boldsymbol{r})\rho(\boldsymbol{r}')}{|\boldsymbol{r} - \boldsymbol{r}'|}d\boldsymbol{r}d\boldsymbol{r}' + G[\rho] = J[\rho] + G[\rho], \tag{3.11}$$

where $J[\rho]$ is the classical Coulomb energy and $G[\rho]$ is a universal functional [8].

3.2 Kohn-Sham approach

Kohn and Sham (KS) developed out of the HK theorems methods for treating an inhomogeneous system of interacting electrons, the so called Kohn-Sham equations [9]. These are self-consistent equations like the Hartree-Fock equations, but the exchange and correlation effects are contained in an appropriate way. We start with the ground state energy written in the form

$$\begin{aligned} E[\rho] &= \int \rho(\boldsymbol{r})\hat{V}_{ext}(\boldsymbol{r})d\boldsymbol{r} + \frac{1}{2}\int \frac{\rho(\boldsymbol{r})\rho(\boldsymbol{r}\,')}{|\boldsymbol{r}-\boldsymbol{r}\,'|}d\boldsymbol{r}d\boldsymbol{r}\,' + G[\rho] \\ &= E_{ext}[\rho] + J[\rho] + G[\rho], \end{aligned} \tag{3.12}$$

and want to derive equations, which are analogous to single particle equations, that are easier to solve. We approximate $G[\rho]$ in the following way

$$G[\rho] = T_s[\rho] + E_{xc}[\rho]. \tag{3.13}$$

$T_s[\rho]$ is the kinetic energy of a system of non-interacting electrons (the s always denotes the system of non-interacting particles, which here serves as reference system so that $(-\frac{\hbar^2}{2m}\nabla^2 + V_s)\phi_i = \epsilon_i\phi_i$)

$$T_s[\rho] = -\frac{\hbar^2}{2m}\sum_{i=1}^{N}\langle\phi_i|\nabla_i^2|\phi_i\rangle, \tag{3.14}$$

where ϕ_i are the Kohn-Sham-orbitals, so that the following is true (when choosing an appropriate V_s)

$$\rho_s(\boldsymbol{r}) = \sum_{i=1}^{N}|\phi_i(\boldsymbol{r})|^2 = \rho_0(\boldsymbol{r}), \tag{3.15}$$

with the exact ground state density $\rho_0(\boldsymbol{r})$ of the interacting system. $E_{xc}[\rho]$ is the exchange-correlation energy of an interacting system. We now have defined all our terms (except E_{xc}, for this see chapter 3.3), which means we can use the variational principle with the energy of the form

$$E^{KS}[\rho] = T_s[\rho] + E_{ext}[\rho] + J[\rho] + E_{xc}[\rho], \tag{3.16}$$

and the constraint that the ϕ_i should be normalized one obtains

$$\delta\left[E^{KS} - \sum_i \epsilon_i(\langle\phi_i|\phi_i\rangle - 1)\right] = 0, \tag{3.17}$$

where ϵ_i is a Lagrange multiplier. This yields the Kohn-Sham equations

$$\left[-\frac{\hbar^2}{2m}\nabla^2 + \left(\int \frac{\rho(\boldsymbol{r}\,')}{|\boldsymbol{r}-\boldsymbol{r}\,'|}d\boldsymbol{r}\,' + V_{xc}(\boldsymbol{r}) + V_{ext}(\boldsymbol{r})\right)\right]\phi_i(\boldsymbol{r}) = \epsilon_i\phi_i(\boldsymbol{r}), \tag{3.18}$$

where

$$V_{xc}(\boldsymbol{r}) = \frac{\delta E_{xc}}{\delta \rho}. \tag{3.19}$$

Now we have to solve single-particle equations for all the ϕ_i's, which actually describe quasi-particles with their energies ϵ_i. But by construction it is guaranteed, that the density of these quasi-particles is equal to the true electron density. As these equations need to be solved self consistently, we first need to assume a starting density ρ_0, construct the Hamiltonian and then find a new density ρ_1 by solving the single particle equations. The procedure has to be done again with ρ_1, and so forth, as long as $|\rho_n - \rho_{n+1}| < \delta_{tol}$. The solution procedure for this is shown in figure 3.1.

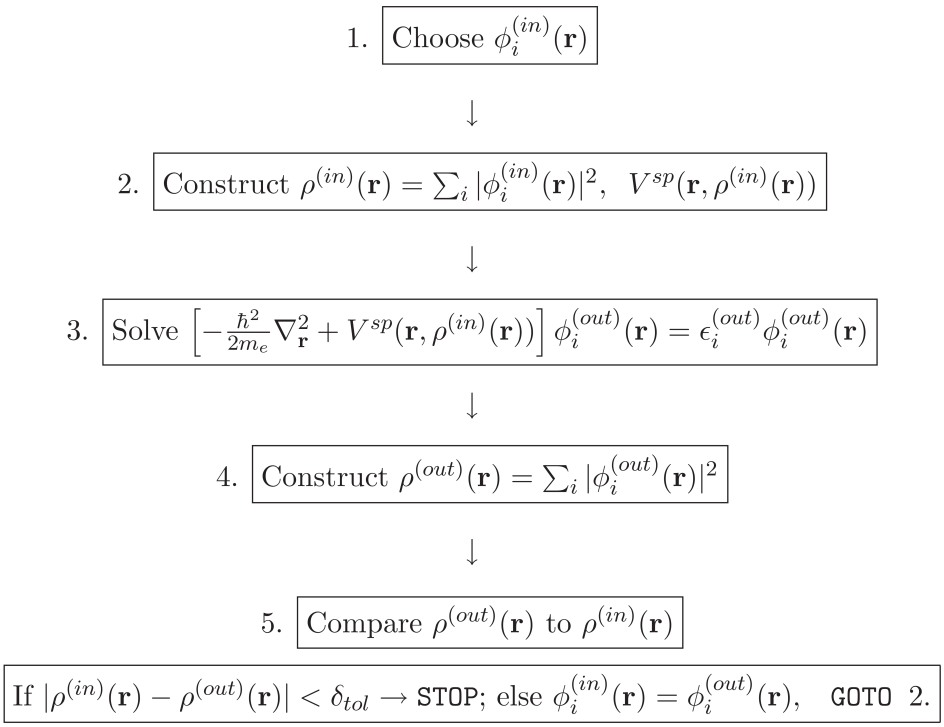

Figure 3.1: Solution process for Kohn-Sham equations [7]

3.3 Exchange-Correlation functional

Until now, no approximations have been made, apart from the BO-approximation, but the exchange-correlation energy E_{xc} is unknown and hence the search for functionals is central in DFT-research. The Kohn-Sham approach is exact, but now we need approximations for E_{xc}, to make our theory really applicable. Two different exchange-correlation functionals will be presented, which are extensively used in calculations.

3.3.1 Local Density Approximation

For a slow varying density $\rho(\boldsymbol{r})$, $E_{xc}[\rho]$ can be written as

$$E_{xc}^{LDA}[\rho] = \int \rho(\boldsymbol{r})\epsilon_{xc}^{HEG}(\rho(\boldsymbol{r}))d\boldsymbol{r}, \tag{3.20}$$

with $\epsilon_{xc}^{HEG}(\rho(\boldsymbol{r}))$ being the exchange-correlation energy density (energy per electron) of a uniform electron gas of density ρ [9]. This we call the Local Density Approximation (LDA), because the dependence of the functional on the density is only local. $\epsilon_{xc}^{HEG}(\rho(\boldsymbol{r}))$ is a function of ρ and we obtain an exchange-correlation potential of the form

$$V_{xc}^{LDA}(\boldsymbol{r}) = \frac{\delta E_{xc}}{\delta \rho} = \epsilon_{xc}^{HEG}(\rho(\boldsymbol{r})) + \rho(\boldsymbol{r})\frac{\partial \epsilon_{xc}^{HEG}(\rho(\boldsymbol{r}))}{\partial \rho(\boldsymbol{r})}. \tag{3.21}$$

> *The exchange-correlation energy due to a particular density $\rho(\boldsymbol{r})$ could be found by dividing the material in infinitesimally small volumes with a constant density. Each such volume contributes to the total exchange correlation energy by an amount equal to the exchange correlation energy of an identical volume filled with a homogeneous electron gas, that has the same overall density as the original material has in this volume* [2].

An exacter derivation of $E_{xc}^{LDA}[\rho]$ can be found in [4]. An astonishing fact is that the LDA not only works for systems with a slowly varying density. It is surprisingly accurate for realistic systems, but it fails in systems that are dominated by electron-electron interaction effects (like heavy fermion systems), because there is no resemblance to a uniform electron gas [11].

3.3.2 Generalized Gradient Approximation

A first step to improve LDA, is to take not only the local density into account, but also the density of the neighbouring volumes. Therefore ϵ_{xc} depends on the gradient of the density, and it is called the Generalized Gradient Approximation (GGA). The exchange-correlation energy is now of the form

$$E_{xc}^{GGA}[\rho] = \int \rho(\boldsymbol{r})\epsilon_{xc}(\rho(\boldsymbol{r}), \nabla\rho(\boldsymbol{r}))d\boldsymbol{r}, \tag{3.22}$$

where $\epsilon_{xc} \neq \epsilon_{xc}^{HEG}$, is a function, that depends on the density $\rho(\boldsymbol{r})$ and the gradient of the density $\nabla\rho(\boldsymbol{r})$. One can choose ϵ_{xc} in different ways, to get different GGA's. This freedom does not exist for LDA, because there is only one correct expression for ϵ_{xc}^{HEG}. In particular, GGA's used in physics focus on exact constraints, whereas in quantum chemistry, parameters are fitted on examined molecules. The most appropriate and most reliable GGA's were proposed in 1996 by Perdew, Burke and Ernzerhof (GGA-PBE) [3].

3.4 Basis sets

The final step in DFT is, that one needs to solve equations of the form

$$\hat{H}_{sp}\phi_i = \epsilon_i\phi_i, \tag{3.23}$$

where $\hat{H}_{sp}$ is the single particle Hamiltonian. In the case of DFT $\hat{H}_{sp}$ is given through equation 3.18 and ϕ_i are the Kohn-Sham single-particle orbitals. The solution process is equivalent for DFT or Hartree-Fock, so the mathematical techniques are the same to solve them.
In general, one first needs to define a ground state density. But before we can define a density, we need a basis set ϕ_p^b, so that we can express the wave function as a linear combination of the basis functions

$$\phi_i = \sum_{p=1}^{P} c_p^i \phi_p^b, \tag{3.24}$$

because we do not know how the ϕ_i's look like, which define the density. Solving now means, that we want to find the coefficients c_p^i, so that our wave function is a linear combination of the basis functions. To exactly define the ϕ_i, one needs an infinite basis set (number of P is infinite), because the ϕ_i belong to a function space with infinite dimension. As this is not practical, we therefore limit the number P, but accept, that we can only generate functions which are close to the exact ϕ_i. Having chosen a basis, the problem reduces to an eigenvalue problem of linear algebra (for further details see [2]). Before we introduce a basis, we want to know, which properties define a good basis.
If we choose a basis set, that is similar to the ϕ_i, the number P reduces in equation 3.24, but we can still accuratly describe the wave function (efficiency). This assumes, that one already knew the solution right before starting the calculation, which is good for few special systems, with the same properties, but for the majority they will poorly describe it. So the basis set should work for the majority of problems (unbiased).
In general, two different basis sets exist, which are mixed to combine their good properties. One are the plane waves, which accuratly describe weakly bound/free electrons and the other ones are local orbitals/atomic like functions, which accuratly describe heavily bound electrons.

3.4.1 Plane waves and pseudopotential method

As already said, the basis set should be efficient and unbiased. Additionally it would be nice, if the basis functions are mathematically simple. Solids or crystals have a periodic structure and hence a periodic Hamiltonian and so we can choose the basis set to be plane waves. The wave function writes

$$\phi_{\boldsymbol{k}}^n(\boldsymbol{r}) = \sum_{\boldsymbol{K}} c_{\boldsymbol{K}}^{n,\boldsymbol{k}} \exp(i(\boldsymbol{k}+\boldsymbol{K})\boldsymbol{r}). \tag{3.25}$$

In this notation, $i = (n, \boldsymbol{k})$ and $p = \boldsymbol{k} + \boldsymbol{K}$. As one can see, this basis-set is $\boldsymbol{k}$-dependent. That means, that one has for different n and same $\boldsymbol{k}$, the same basis set, but for different $\boldsymbol{k}$ one has another basis set. Rememeber that we have to limit our basis set. We choose $K \leq K_{max}$, that corresponds to a sphere with radius $R = K_{max}$ around the origin of reciprocal space. All reciprocal lattice vectors, smaller than K_{max} are taken into the basis set.
Determining the eigenvalue problem, yields for each eigenvalue $\epsilon^{n,\boldsymbol{k}}$ an eigenvector $[c_{\boldsymbol{K}}^{n,\boldsymbol{k}}]_{P\times 1}$ of P values for $c_{\boldsymbol{K}}^{n,\boldsymbol{k}}$ corresponds [2]. The P eigenvalues each with their own set of coefficients, and each leading to another eigenfunction $\phi_{\boldsymbol{k}}^{n}$. So we found P different eigenfunctions, all with the same $\boldsymbol{k}$ but with different band index n. When we repeat the calculations for every $\boldsymbol{k}$, that is contained in the first Brillouin zone, we get the band structure. The number of $\boldsymbol{k}$'s defines the sampling. So far, so good. The problem is, that we would need about 10^8 plane waves [2] for realization and this is way beyond practice.
To make this ansatz applicable, we look at the wave function of a simple atom. The most oscillating part is near the nucleus, so one needs to modify something in this region. One can use atomic like functions in combination with plane waves (APW-method, see chapter 3.4.2), or one can modify the potential (pseudopotential method).
As already said, the wave function oscillates in the inner region, outside the electrons are almost free. Chemistry happens in the outer shells, and for the description in the inner shells, we replace the potential through a pseudopotential, to reach smooth tails of the wave functions there. Going to the outer region, the potential evolves into the true potential. Using this ansatz, we *only* need about 270 plane waves [2], which is a managable amount.
Two criteria are important, when defining a pseudopotential (transferability and softness). First one is, that it can be used in a lot of environments (molecules, solids, etc.) and the second one is, that we only will need few plane waves because of this potential.

3.4.2 Augmented plane waves

Even though the pseudopotential method is useful, one cannot appropriately describe properties of the system near the nucleus. We have to search for another basis set, that describes the electrons properly, which means they are more or less *free* far away from the nuclei and near the nuclei they behave as bound to an atom. Therefore we use a combination of plane waves and atomic like functions. For this we divide the space into two regions. The so called muffin tin sphere S_α with radius R_α around each atom, and the remaining space outside of them called the interstitial region I. The augmented plane wave (APW) basis set is defined as in Ref. [2]

$$\phi_{\boldsymbol{K}}^{\boldsymbol{k}}(\boldsymbol{r}, E) = \begin{cases} \frac{1}{\sqrt{V}} \exp(i(\boldsymbol{k}+\boldsymbol{K})\boldsymbol{r}), & \boldsymbol{r} \in I \\ \sum\limits_{l,m} A_{lm}^{\alpha,\boldsymbol{k}+\boldsymbol{K}} u_l^\alpha(r', E) Y_m^l(\theta', \phi'), & \boldsymbol{r} \in S_\alpha \end{cases} \tag{3.26}$$

The position inside the spheres is given with respect to the center of each sphere by $\boldsymbol{r}' = \boldsymbol{r} - \boldsymbol{r}_\alpha$ (see figure 3.2). $u_l^\alpha(r', E)$ are the solutions of the radial part of the Schrödinger equation for

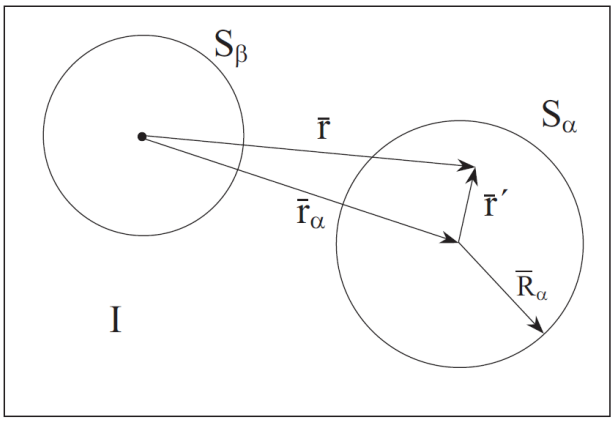

Figure 3.2: Division of a unit cell in muffin tin regions S_α and the interstitial region I [2]

a free atom α and $Y_m^l(\theta', \phi')$ are spherical harmonics. In S_α the basis is a linear combination of atomic functions ($A_{lm}^{\alpha,\boldsymbol{k}+\boldsymbol{K}}$ are coefficients) and should therefore be close to the actual eigenfunctions, so that they appropriately describe the system. One requirement is that the plane waves match the atomic functions in value, over the complete surface of the sphere, in order to determine the coefficients uniquely.
As for plane waves we have to limit the basis, which is in principle infinite and hence we introduce a l_{max} to limit their number. The cut off parameter for plane waves was K_{max}. In order to match these limitations, we compare the number of nodes per unit length which yields $R_\alpha K_{max} = l_{max}$. We accept therefore, that the matching at the boundaries are not exact, but sufficient. To visualize the basis set, imagine an oscillating function, that changes into something more complex inside of S_α.
To describe the eigenstates accurately with this basis one needs to set the free parameter E, in $u_l^\alpha(r', E)$, equal to the band energy $\epsilon_{\boldsymbol{k}}^n$ and therefore we have to start with a guessed value for $\epsilon_{\boldsymbol{k}}^n$ before we start solving the secular equation (see figure 3.3). We will need about 131 APW's so that the diagonalization is much faster, but we only find one eigenvalue and not P simultaneously as for plane waves and hence this method is in total slower than the pseudopotential method.

3.4.3 Linearized Augmented Plane Waves

The regular LAPW method: The APW method contains one difficulty, as we do not know the eigenenergies $E = \epsilon_{\boldsymbol{k}}^n$ yet, to construct the basis set, because this is what we are actually searching for. For this the basis of Linearized Augmented Plane Waves (LAPW) exists in order to circumvent this obstacle.

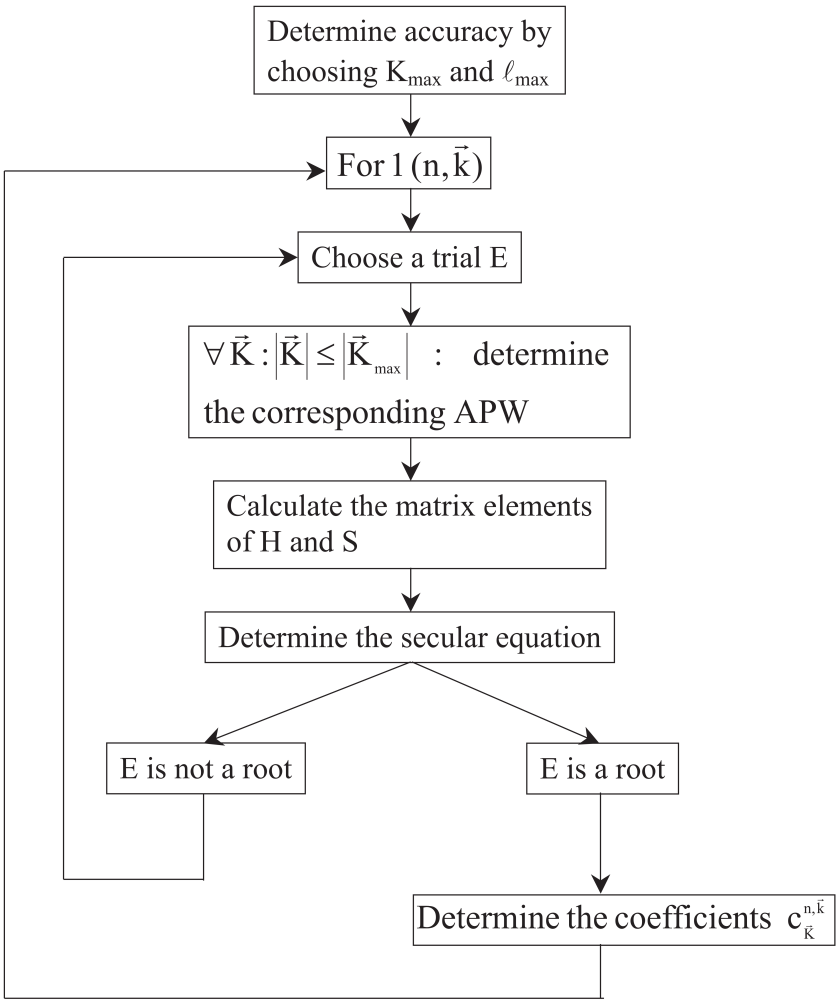

Figure 3.3: Flowchart of the APW method [2]

We make a Taylor expansion of $u_l^\alpha(r', E)$ around a specific energy E_0

$$u_l^\alpha(r', \epsilon_{\boldsymbol{k}}^n) = u_l^\alpha(r', E_0) + (E_0 - \epsilon_{\boldsymbol{k}}^n) \left.\frac{\partial u_l^\alpha(r', E)}{\partial E}\right|_{E=E_0} + \mathcal{O}\left[(E_0 - \epsilon_{\boldsymbol{k}}^n)^2\right], \tag{3.27}$$

and take the first two terms into account, to create the LAPW basis

$$\phi_{\boldsymbol{K}}^{\boldsymbol{k}}(\boldsymbol{r}, E) = \begin{cases} \frac{1}{\sqrt{V}} \exp(i(\boldsymbol{k} + \boldsymbol{K})\boldsymbol{r}), & \boldsymbol{r} \in I \\ \sum\limits_{l,m} (A_{lm}^{\alpha,\boldsymbol{k}+\boldsymbol{K}} u_l^\alpha(r', E_0) + B_{lm}^{\alpha,\boldsymbol{k}+\boldsymbol{K}} \dot{u}_l^\alpha(r', E_0)) Y_m^l(\theta', \phi'), & \boldsymbol{r} \in S_\alpha \end{cases} \tag{3.28}$$

where $\dot{u}_l^\alpha = \left.\frac{\partial u_l^\alpha(r', E)}{\partial E}\right|_{E=E_0}$. An additional coefficient must be introduced, because we do not know the energy difference $E_0 - \epsilon_{\boldsymbol{k}}^n$. To determine $A_{lm}^{\alpha,\boldsymbol{k}+\boldsymbol{K}}$ and $B_{lm}^{\alpha,\boldsymbol{k}+\boldsymbol{K}}$ we need the matching,

at the sphere boundary, to the plane waves in value and slope. In order to accurately describe the band structure, we should choose a set of $E^{\alpha}_{1,l}$ (for every band l) and not an universal E_0. The LAPW basis thus is

$$\phi^{\boldsymbol{k}}_{\boldsymbol{K}}(\boldsymbol{r}, E) = \begin{cases} \frac{1}{\sqrt{V}} \exp(i(\boldsymbol{k}+\boldsymbol{K})\boldsymbol{r}), & \boldsymbol{r} \in I \\ \sum\limits_{l,m} (A^{\alpha,\boldsymbol{k}+\boldsymbol{K}}_{lm} u^{\alpha}_{l}(r', E^{\alpha}_{1,l}) + B^{\alpha,\boldsymbol{k}+\boldsymbol{K}}_{lm} \dot{u}^{\alpha}_{l}(r', E^{\alpha}_{1,l})) Y^{l}_{m}(\theta', \phi'), & \boldsymbol{r} \in S_{\alpha} \end{cases} \tag{3.29}$$

With this basis we get, out of one diagonalization, P different band energies for one single $\boldsymbol{k}$, as for plane waves. The limitation criteria here is the product $R^{min}_{\alpha} K_{max}$, where R^{min}_{α} is the smallest muffin tin radius. A smaller K_{max} yields a smaller matrix size and a larger R^{min}_{α} reduces computation time and hence $R^{min}_{\alpha} K_{max}$ should be kept constant. The basis set size is then about 195 basis functions. As the calculation time scales with the third power of the basis set size, this method is 2-3 times faster than plane waves [2].

LAPW with Local Orbitals: A well bound electron to the nucleus is called a core state and participates not in chemical bonding. It is therefore contained in the muffin tin sphere. States outside the sphere take part in chemical bonding and are called valence states and are treated by LAPW. Low lying valence states are called semi-core states. If we want to describe these, we do not know how to choose $E^{\alpha}_{1,l}$, because we do not know in which band these states sit. We add another type of basis function to LAPW, a local orbital (LO), to solve this dilemma

$$\phi^{lm}_{\alpha,\mathrm{LO}}(\boldsymbol{r}, E) = \begin{cases} 0, & \boldsymbol{r} \notin S_{\alpha} \\ (A^{\alpha,LO}_{lm} u^{\alpha}_{l}(r', E^{\alpha}_{1,l}) + B^{\alpha,LO}_{lm} \dot{u}^{\alpha}_{l}(r', E^{\alpha}_{1,l}) + C^{\alpha,LO}_{lm} u^{\alpha}_{l}(r', E^{\alpha}_{2,l})) Y^{l}_{m}(\theta', \phi'), & \boldsymbol{r} \in S_{\alpha} \end{cases} \tag{3.30}$$

Its name comes from the fact, that an LO acts only in the region of one particular atom S_{α}. There is no $\boldsymbol{k}$- or $\boldsymbol{K}$-dependence, because they have no connection to plane waves. The energies $E^{\alpha}_{1,l}$ and $E^{\alpha}_{2,l}$ correspond to the next highest or the next lowest valence state in relation to the mentioned semi-core state. The coefficients $A^{\alpha,LO}_{lm}$, $B^{\alpha,LO}_{lm}$ and $C^{\alpha,LO}_{lm}$ are determined by normalization and matching of zero value and zero slope at the boundary. Through this additional function, the basis set size and thus computational time increase, but the accuracy is much better [2].
A few more types of basis sets exist, such as the APW+lo, which combines the good features of APW and LAPW+LO. As this would lead too far, those are not explained here, but in [2].

4 Properties of Graphene

Carbon atoms have a chemical configuration of [He] $2s^2$ $2p^2$ and hence they can form various complex molecules. A really interesting and today often used and discussed material is graphene. Because of its structure, it is light as well as robust. For a long time, the production of single layer graphene was a very time-consuming procedure, but since 2014 one can produce large quantities of defect-free graphene [15].
Moreover it has some interesting physical properties, such as a remarkably high electron mobility ($> 15000\ \frac{\mathrm{cm}^2}{\mathrm{Vs}}$). Often it is used in spintronics, because carbon has nearly no nuclear magnetic moment and because of its small spin-orbit coupling (SOC) [20], it is theoretically expected to have long spin-lifetimes, which is good, when transporting spin information. Here one will get a short introduction of important properties of graphene.

4.1 Lattice

The carbon atoms in graphene have a sp^2-hybridisation and hence every atom can have three equal σ-bondings to other carbon atoms. This is why the graphene lattice has the honeycomb or hexagonal two-dimensional form (see figure 4.1). Graphene belongs to the point group D_{6h} which has 24 symmetry operations (see figure A.1). The distance between the carbon atoms is $a_C = 1.42$ Å. The last non hybridized p_z-orbitals, which are orthogonal to the graphene plane, form a π-bonding system. The primitive cell is formed by the lattice unit vectors $\boldsymbol{a}_1$ and $\boldsymbol{a}_2$

$$\boldsymbol{a}_1 = \frac{a_C}{2}\left(3, \sqrt{3}\right), \qquad \boldsymbol{a}_2 = \frac{a_C}{2}\left(3, -\sqrt{3}\right), \tag{4.1}$$

where $a = |\boldsymbol{a}_1| = |\boldsymbol{a}_2| = \sqrt{3}a_C \approx 2.46$ Å. The reciprocal lattice unit vectors $\boldsymbol{b}_1$ and $\boldsymbol{b}_2$ are given by

$$\boldsymbol{b}_1 = \frac{2\pi}{3a_C}\left(1, \sqrt{3}\right), \qquad \boldsymbol{b}_2 = \frac{2\pi}{3a_C}\left(1, -\sqrt{3}\right), \tag{4.2}$$

which can be found by using the relation $\boldsymbol{a}_i \cdot \boldsymbol{b}_j = 2\pi\delta_{ij}$ and also form a hexagonal reciprocal lattice.

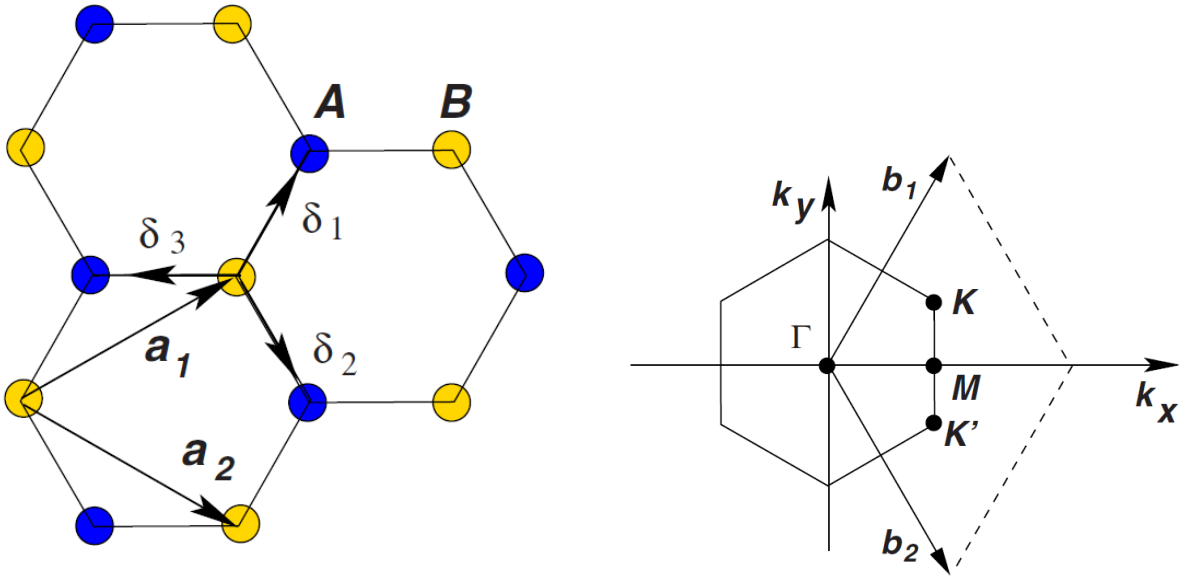

(a) Lattice structure of graphene. $\boldsymbol{a}_1$ and $\boldsymbol{a}_2$ are the lattice unit vectors, and $\delta_i, i = 1, 2, 3$ are the nearest-neighbour vectors

(b) Corresponding Brillouin zone. The Dirac cones are located at the K and K' points. $\boldsymbol{b}_1$ and $\boldsymbol{b}_2$ are the reciprocal lattice unit vectors

Figure 4.1: Lattice and reciprocal lattice of graphene [13]

4.2 Band structure

The band structure of graphene can be calculated, using the tight-binding approximation (TBA)

$$E_{\pm}(\boldsymbol{k}) = \pm t \cdot \sqrt{3 + f(\boldsymbol{k})} + t' f(\boldsymbol{k}) \tag{4.3}$$

with

$$f(\boldsymbol{k}) = 4\cos\left(\frac{\sqrt{3}k_y a}{2}\right)\cos\left(\frac{3k_x a}{2}\right) + 2\cos\left(\sqrt{3}k_y a\right) \tag{4.4}$$

where $a = 2.46$ Å is the lattice constant, $t = 2.7$ eV is the nearest neighbour hopping energy and t' is the next nearest neighbour hopping energy ($0.02t \leq t' \leq 0.2t$) [13]. The band structure is shown in figure 4.2, where one can clearly see, that the upper (π^*) and the lower (π) band touch each other at six points (actually there is a band gap at the order of 10^{-6} eV, when SOC is turned on [20]), namely the K and K' points from figure 4.1, the so called Dirac points. As there are two atoms per unit cell, there are in general two nondegenerate low energy eigenstates. The lower band can be exactly filled with 2 valence electrons at temperature $T = 0$, and thus the Fermi energy $E_F = 0$, which means, that graphene has electron-hole symmetry. Pure graphene is therefore a zero gap semiconductor (or zero-overlap semimetal).

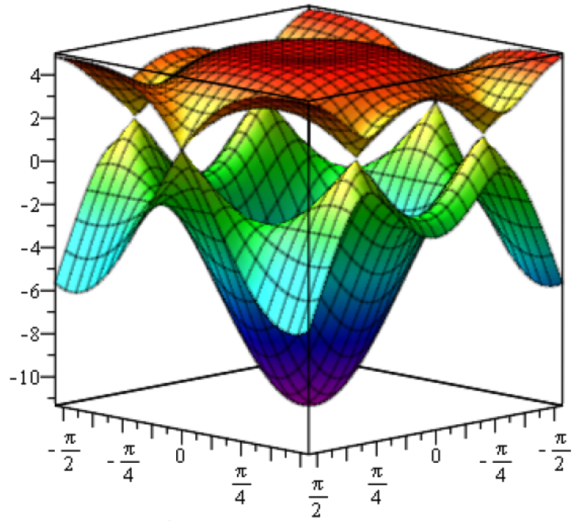

(a) Upper (π^*) and lower (π) band for $t = 2.7$ eV and $t' = 0.2t$. Axis: k_x, k_y and E [eV]

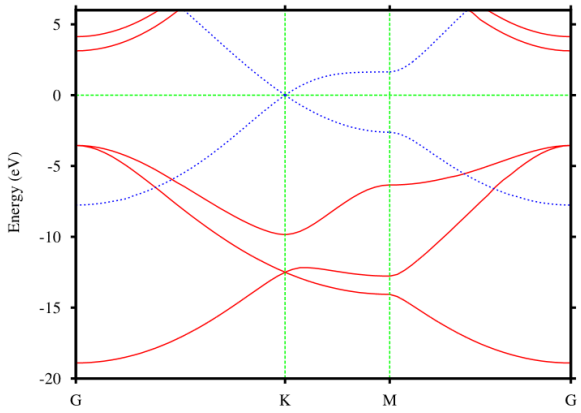

(b) Band structure of a single graphene layer. Solid red lines are σ-bands and dotted blue lines are π-bands [14]

Figure 4.2: Theoretical band structure of graphene

4.3 Closer look on Dirac points

Taking a closer look on the Dirac points, the dispersion in the low energy limit can be obtained by expanding the formula for the band structure around $K = \left(\frac{2\pi}{3a}, \frac{2\pi}{3\sqrt{3}a}\right)$ with $\boldsymbol{k} = \boldsymbol{K} + \boldsymbol{q}$ and $|\boldsymbol{q}| \ll |\boldsymbol{K}|$

$$E_{\pm}(\boldsymbol{q}) = \pm v_F |\boldsymbol{q}| + \mathcal{O}\left[\left(\frac{q}{k}\right)^2\right], \tag{4.5}$$

where $\boldsymbol{q}$ is the momentum relative to the Dirac point and $v_F = \frac{3ta}{2} \approx 1 \cdot 10^6 \frac{\mathrm{m}}{\mathrm{s}}$ is the Fermi velocity [13]. Note, that in this limit the velocity does not depend on momentum or energy, as usual. An expansion around K and taking t' into account up to the second order in $\frac{q}{K}$ yields

$$E_{\pm}(\boldsymbol{q}) = 3t' \pm v_F |\boldsymbol{q}| - \left(\frac{9t'a^2}{4} \pm \frac{3ta^2}{8} \sin(3\theta_q)\right) |\boldsymbol{q}|^2, \tag{4.6}$$

where $\theta_q = \arctan\left(\frac{q_x}{q_y}\right)$ is the angle in momentum space. Remark, that t' breaks the electron hole symmetry, and the bands become asymmetric with respect to the Fermi energy. The energy dispersion 4.5 is close to the one of massless relativistic particles, which are described by the Dirac equation. It follows, that the cyclotron mass is proportional to the square root of the electronic density ρ

$$m^* = \frac{\sqrt{\pi}}{v_F} \sqrt{\rho}, \tag{4.7}$$

which provides evidence of massless Dirac quasi-particles (Dirac fermions) in graphene [13]. As already said, the electron wave function near the Dirac points (this case is for K) obey a 2D Dirac equation

$$-iv_F\boldsymbol{\sigma}\cdot\nabla\Psi(\boldsymbol{r}) = E\Psi(\boldsymbol{r}), \tag{4.8}$$

$$\Psi_{\pm,\boldsymbol{K}}(\boldsymbol{k}) = \frac{1}{\sqrt{2}}\begin{pmatrix}\exp(-i\theta_{\boldsymbol{k}}/2)\\ \pm\exp(i\theta_{\boldsymbol{k}}/2)\end{pmatrix}, \qquad H_K = v_F\boldsymbol{\sigma}\boldsymbol{k}, \qquad E = \pm v_F k, \tag{4.9}$$

with the Pauli spin-matrices $\boldsymbol{\sigma} = (\sigma_x, \sigma_y)$. The signs $\pm$ correspond to the eigenenergies $E = \pm v_F k$ in the π^* and π bands. A similar equation exists for the K' Dirac point. The wave functions of these two are related by time-reversal symmetry. One can now show, that the helicity, defined by the operator

$$\hat{h} = \frac{1}{2}\boldsymbol{\sigma}\cdot\frac{\boldsymbol{p}}{|\boldsymbol{p}|} \tag{4.10}$$

is a good quantum number close to the Dirac points [13].

4.4 Density of States

The density of states per unit cell is given by

$$\rho(E) = \frac{4|E|}{\pi^2 t^2\sqrt{Z_0}}\cdot \mathrm{F}\left(\frac{\pi}{2}, \sqrt{\frac{Z_1}{Z_0}}\right), \tag{4.11}$$

with

$$Z_0 = \begin{cases} \left(1+\frac{|E|}{|t|}\right)^2 - \frac{[(E/t)^2-1]^2}{4}, & -t \le E \le t \\ 4\frac{|E|}{|t|}, & t \le |E| \le 3t \end{cases} \tag{4.12}$$

and $Z_0 = Z_1$, but with interchanged domains [13]. $\mathrm{F}\left(\frac{\pi}{2}, x\right)$ is the complete elliptic integral of the first kind. As the band structure can be approximated at the Dirac point, so can the density of states

$$\rho(E) = \frac{2A_c|E|}{\pi v_F^2}, \tag{4.13}$$

with $A_c = \frac{3\sqrt{3}a^2}{2}$ which is the unit cell area. Figure 4.3 shows the density of states for different t'.

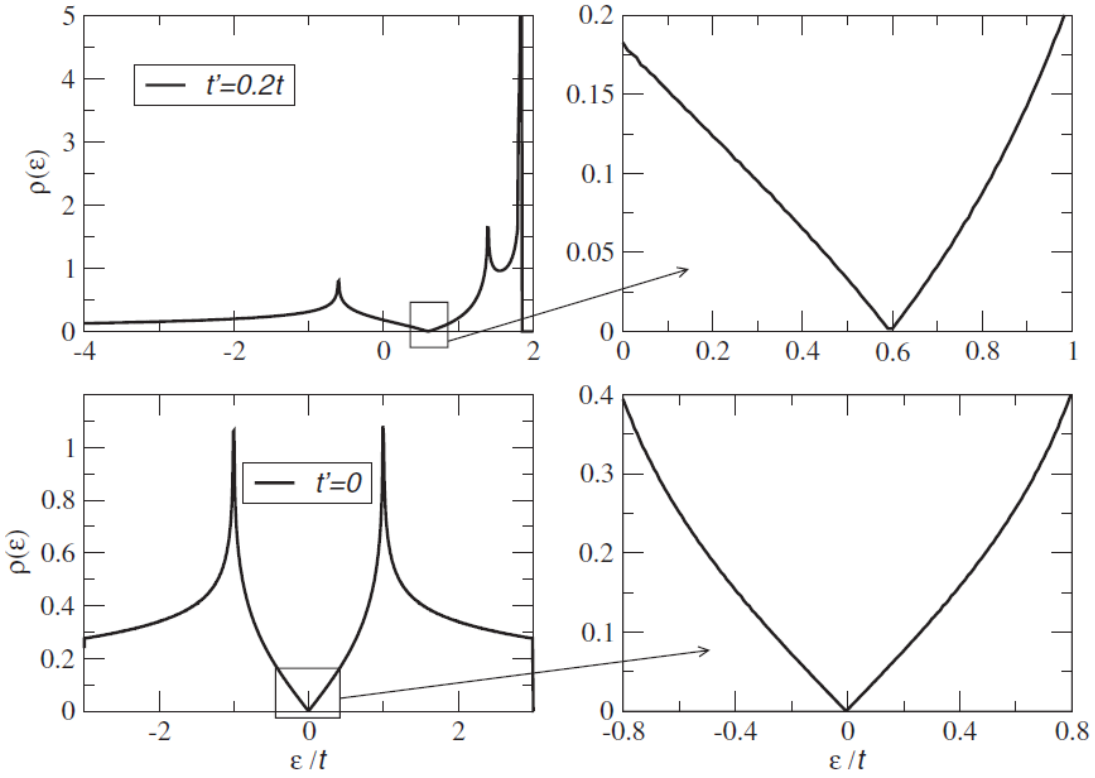

Figure 4.3: Density of states per unit cell [13]

One can see, that the density of states, in the vicinity of the neutrality point, can be approximated by $\rho(E) \propto |E|$. The density of states is vanishing at zero energy and the peaks, left and right of the neutrality point are called van Hove singularities, which refer to the points in k-space, where $|\vec{\nabla}_{\vec{k}} E| = 0$.

5 Single layer graphene

The DFT calculations on graphene were executed with an ab initio (= from the beginning) calculation, implemented in the WIEN2k code [10]. A detailed description of the procedure is given in A.1. In this chapter, the most important results are stated and explained. The main input for the WIEN2k code is the *structure file*, which is given (for graphene) by figure A.1. The lattice parameters are chosen such, that the two dimensional honeycomb structure (see figure 5.1) is obtained, with a vacuum spacing of $28a_0$ along z-direction ($a_0 \approx 0.5$ Å). Hence the overlap of the wave functions in this direction is minimized. The optimal parameters, that were obtained can be seen in A.1. The calculation was performed with $RK = 8$ and k-point sampling (KPTS) of $21 \times 21 \times 1$ for the band structure and $RK = 8$ and k-point sampling of $42 \times 42 \times 1$ for the DOS. Remember that RK is the cut-off parameter, which limits the basis set size, to have a good compromise between duration and accuracy of the calculation. The k-point sampling also defines the accuracy of the calculation. In general it is valid to say, the more k-points the better, but the duration also scales linearly with the number of k-points.
As the calculation has to be performed in a self-consistent way, one first needs a starting density ρ_0. It is constructed by taking the superposition of atomic densities [10].

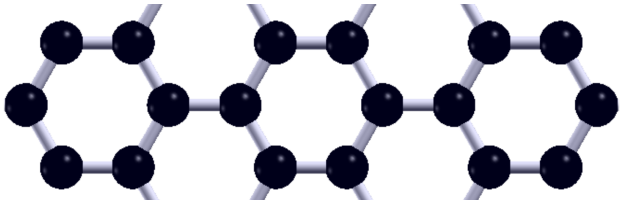

Figure 5.1: Lattice of graphene constructed with Xcrysden (crystalline and molecular structure visualisation program)

5.1 Band structure

The calculated band structure for graphene was plotted along the high symmetry points $\Gamma - M - K - \Gamma$ where the Fermi energy was set to zero (see figure 5.2), which can be compared to the tight-binding structure (figure 4.2). As expected, the upper π^* and the lower π bands touch each other at the K-point, where the dispersion shows linear behaviour.

Moreover the dispersion at the Γ-point shows a parabolic behaviour for energies > 3 eV, which is similar to the dispersion of a free electron gas. This contribution comes from the vacuum spacing between the graphene layers, since this region has to be filled with plane waves.

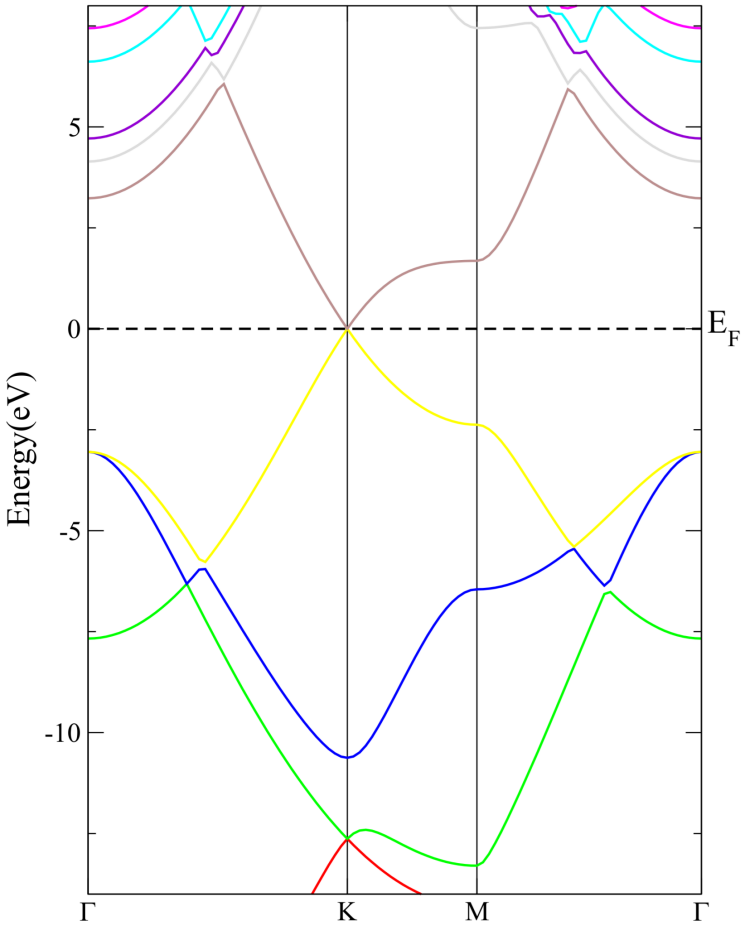

Figure 5.2: Band structure of graphene. π^*-band (brown), π-band (yellow), other bands are σ-bands

5.2 Density of States

The calculated DOS is shown in figure 5.3, which can be compared to the analytical one (figure 4.3). The graph shows the expected behaviour at the neutrality point (see 5.4), where the DOS can be approximated by $\rho(E) \propto |E|$. The different colors refer to different orbitals. Note, that the DOS (black line) is the density of states for the unit cell, whereas the orange line is the one for a single carbon atom. The low lying s and p_x+p_y states are forming the sp^2-hybridisation, which are responsible for the robustness of graphene. In the low

energy region, the main contribution comes from the p_z states, that form the π-bonds, which are responsible for the large conductance. Clearly visible are the van Hove singularities, at around -2.5 eV and 1.7 eV. But these peaks from the p_z contribution do not reach the total DOS value, since orbital contributions are taken from inside muffin tin spheres only. Therefore the main contribution to the DOS at higher energies (> 3 eV) are mainly due to states from the interstitial region.

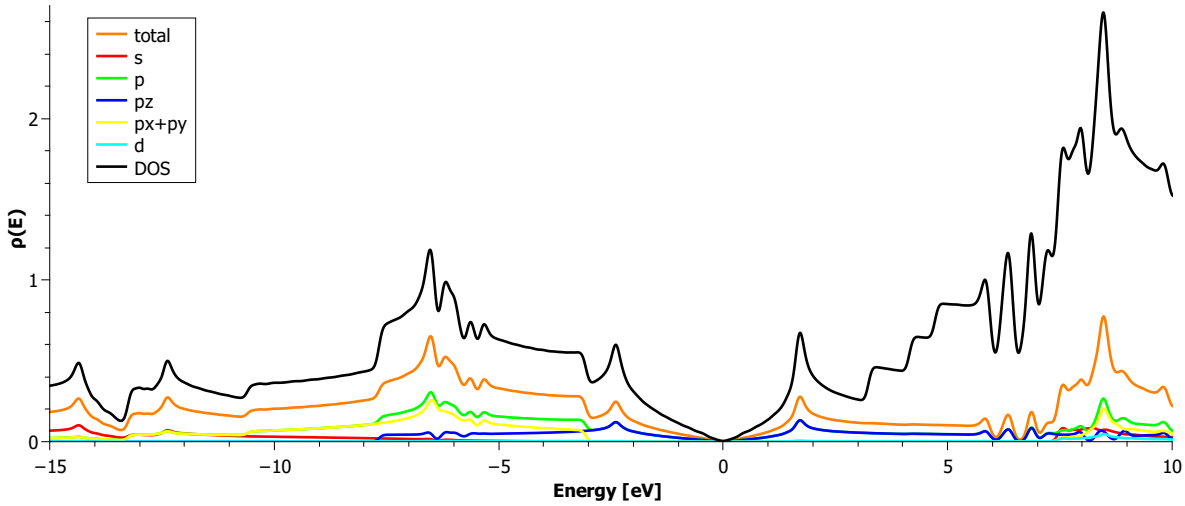

Figure 5.3: Calculated density of states

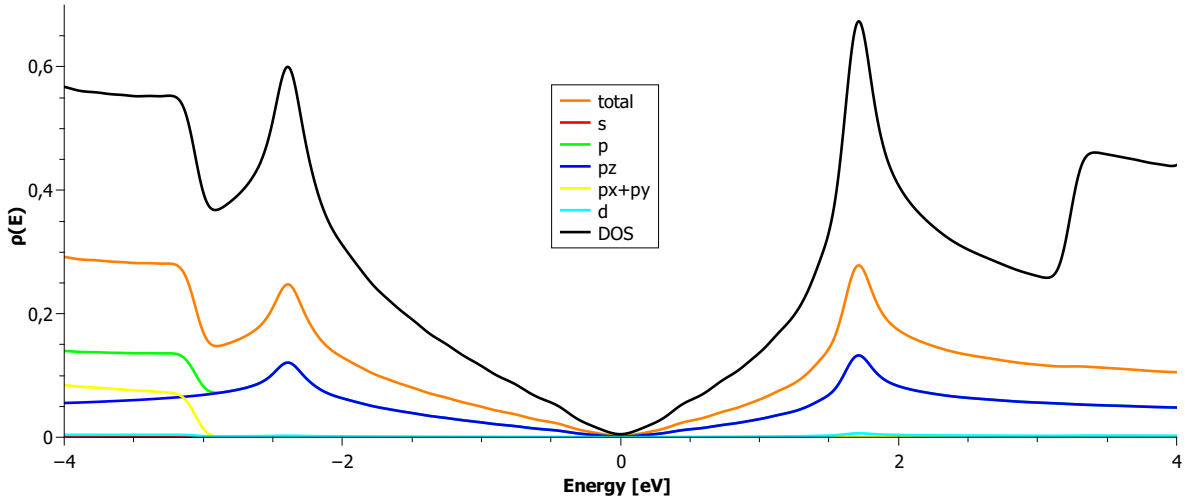

Figure 5.4: Calculated density of states at neutrality point

6 Methylated graphene structure

This part deals with the problem of a modified graphene structure. As one can see in figure 6.1, we added a CH_3 molecule (methyl group) with perpendicular orientation to the graphene layer. A methyl group consists of one carbon atom bonded to three hydrogen atoms and it is often found in organic materials, usually in larger molecules. Thus this structure is called methylated graphene. We chose the molecule, since graphene is expected to be contaminated by organic molecules. In principle it is not clear, where the molecule will bind (top, hollow or bridge position), but we know from the hydrogenated system [20, 17], that the top position is favoured in this case, since carbon and hydrogen have almost the same pauling electronegativity (C: 2.55, H: 2.20 [21]) and thus behave similar. A description of the performed calculations is given in A.1.2. Because of the methyl group, the inversion symmetry is broken and the point group reduces to C_{3v}, which has 6 symmetry operations (see figures A.7,A.8). In order to get the lowest energy configuration, several calculations of different orientations of the molecule should be performed (see figure 6.1). But due to reasons of symmetry, the lowest energy configuration will in principle be such that the carbon-atom, where the molecule is attached to, forms a tetrahedron with the methyl group (see figure 6.2), which is lifted from the graphene layer. Due to the lack of time, we considered (as an approximation) the lattice constant, to be the one of the single layer graphene.

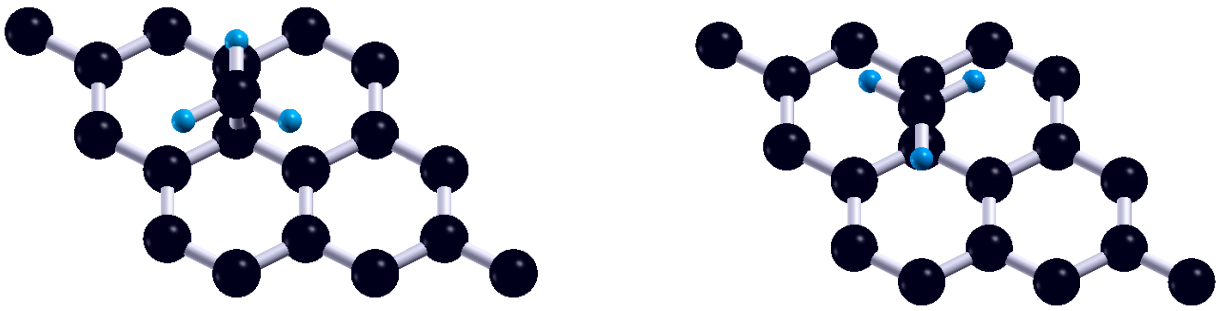

(a) Top configuration

(b) Hollow configuration

Figure 6.1: Different orientations of methyl group with respect to graphene layer

The structural parameters of the tetrahedron obtained from force relaxations are as follows

$$\theta_1 = 106.4° \qquad \theta_2 = 109.9° \qquad \theta_3 = 112.3° \qquad \theta_4 = 109.1°,$$

$$d_1 = 1.099 \text{ Å} \qquad d_2 = 1.588 \text{ Å} \qquad d_3 = 1.505 \text{ Å} \qquad d_4 = 0.426 \text{ Å},$$

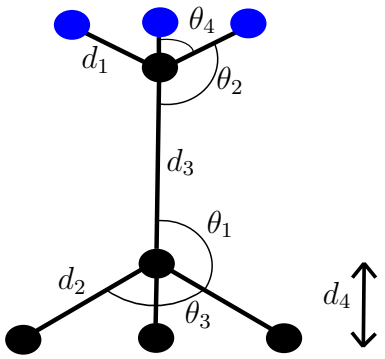

Figure 6.2: Structural parameters of the methyl group

which is close to an ideal sp^3-hybridized tetrahedron with $\theta_{tetrah.} \approx 109.47°$. In contrast to the single layer graphene, where the bonding length between carbon atoms is 1.42 Å , the bonding between the carbon atoms, in this structure, differs from 1.4 Å to 1.43 Å. The task is now to find out, how these change the physical properties of the system. In principle one can for example expect a magnetic moment of the system (spin-polarized calculation) and a gap occurring in the band structure, due to the covalently bonded methyl groups (through C-C bonding) [18]. To obtain the highest accuracy, one has to perform a lot of calculations with different parameter sets (k-points and RK), so that the total energy and the magnetic moment converge. Due to the lack of time, we only considered calculations with RK to be between 3.5 and 4.5 with k-point sampling $5 \times 5 \times 1$. As the total energy for the hollow configuration is lower than the one for the top configuration (see table 6.1), this one will be preferred by the nature and only the results on the hollow configuration are given.

	ENE (3.5)	ENE (4)	ENE (4.5)	FER (3.5)	FER (4)	FER (4.5)
Top		-1451.351	-1451.356		-0.11866	-0.11867
Hollow	-1451.330	-1451.365	-1451.372	-0.11816	-0.11518	-0.11473
ΔE [eV]		0.19	0.22			

Table 6.1: Total energies (ENE) and fermi energies (FER) in units [Ry] for different RK (number in brackets) with KPTS $= 5 \times 5 \times 1$

6.1 Band structure

The calculated band structure for methylated graphene was plotted along the high symmetry points $\Gamma - M - K - \Gamma$ with Fermi level set to zero, where we considered a spin-polarized calculation (see figure 6.3) with $RK = 4$ and k-point sampling $5 \times 5 \times 1$. As one can already see, the Dirac point is no longer at K, but at the Γ-point. This considered 3×3 methylated graphene supercell therefore has properties of the 1×1 graphene unit cell. This is due to the coincidence, that the K-point of this Brillouin zone matches with the Γ-point of the graphene Brillouin zone (see figure 6.4). A spin splitting can be observed and thus a net magnetic moment occurs, since the spin up bands, which sit lower in energy than the spin down bands, are getting filled sooner. One observes an exchange splitting of about 0.5 eV at the Fermi level and also a splitting of the low lying carbon σ-bands. Moreover a gap of about 0.2 eV occured in the band structure at the Γ-point.

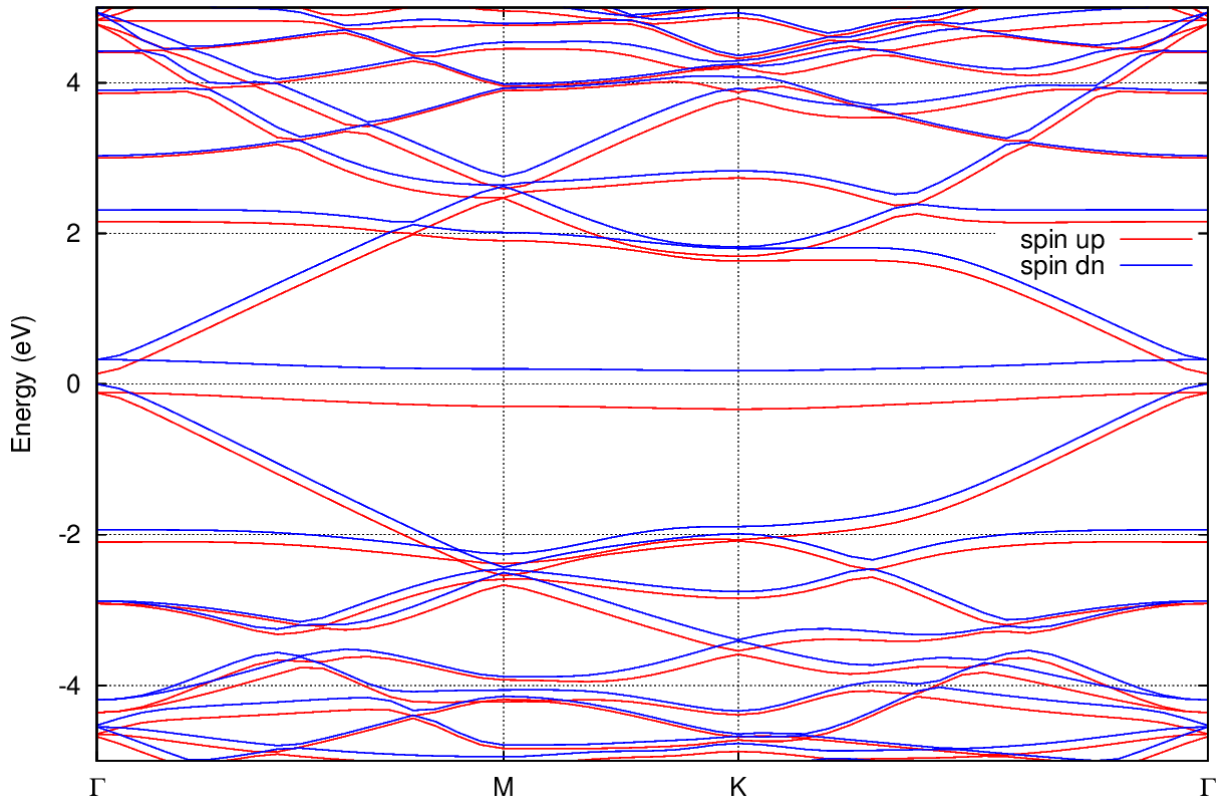

Figure 6.3: Spin resolved band structure of methylated graphene

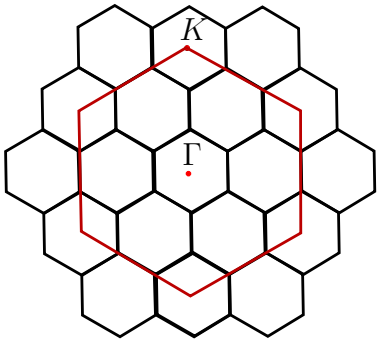

Figure 6.4: Brillouin zone matching

6.2 Magnetization

The total magnetic moment per unit cell is defined as

$$M = (N_\uparrow - N_\downarrow)\mu_B = \int_{-\infty}^{E_F} (g_\uparrow(E) - g_\downarrow(E))\mu_B dE \tag{6.1}$$

where $N_\uparrow$ ($N_\downarrow$) is the number of electrons in the unit cell with spin up (down) and $g_\uparrow(E)$ ($g_\downarrow(E)$) is the DOS per unit cell for spin up (down). We obtained a total spin magnetic moment in the unit cell of 1.00011 μ_B for $RK = 4.5$ and for $RK = 4$ we obtained 0.99993 μ_B. One can say, that there is definetely a magnetic moment as expected, of almost exactly 1 μ_B. This is in agreement to Lieb's theorem [22], since we have one monovalent covalently bonded methyl group on one lattice site. The distribution of the magnetic moments over the unit cell is viewed in figure 6.5.

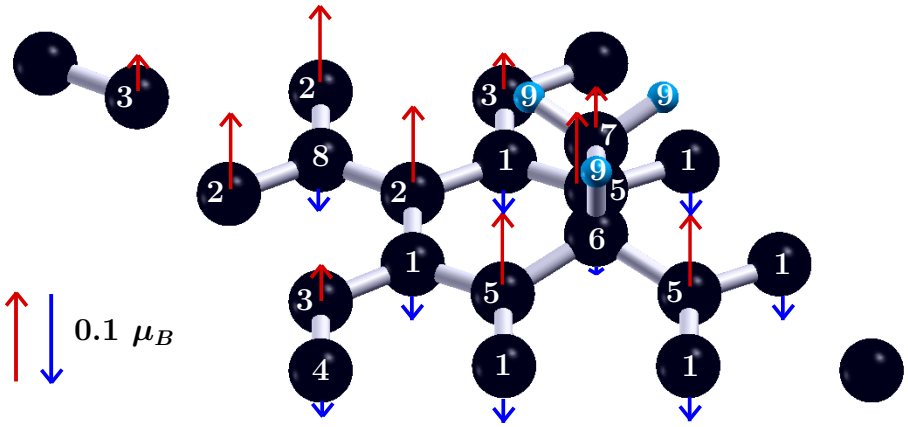

Figure 6.5: Sketch of the spin distribution in the unit cell

Spin down (blue) and spin up (red) are sketched relatively to 0.1 μ_B (long arrows at the left). The spins for the hydrogen atoms are quite small and thus not contained in the sketch. One can clearly see, that the magnetic moments of the sublattices have different sign, but the spin down contribution is less than the spin up contribution and thus the resulting total magnetic moment is about 1 μ_B. Table 6.2 shows the strength of the magnetic moment for the different atoms, defined in A.8, which in sum lead to the total magnetic moment per unit cell, taking the multiplicity into account.

site	magnetic moment [μ_B]	multiplicity	total contribution [μ_B]
interstitial	0.56197	1	0.56199
atom 1	-0.02706	6	-0.16236
atom 2	0.08385	3	0.25155
atom 3	0.03773	3	0.11319
atom 4	-0.01739	1	-0.01739
atom 5	0.08029	3	0.24087
atom 6	-0.00540	1	-0.00540
atom 7	0.04309	1	0.04309
atom 8	-0.02535	1	-0.02535
atom 9	-0.00008	3	-0.00024
total	0.99993	1	0.99993

Table 6.2: Magnetic moments of the single atoms for $RK = 4$

Due to the sp^3 hybridization, which are formed by the methyl admolecules, the spin-orbit coupling will be increased, such that the spin Hall effect could be observed, that offers the possibility of electrically driven spintronics [20].

6.3 Density of states

The calculated atomic resolved DOS (case without spin polarization, $RK = 3.5$ and a k-point sampling of $15 \times 15 \times 1$) is shown in figure 6.6. The numbering of the atoms refers to the one from table 6.2 and figure 6.5.
The peak at the Fermi level indicates an exchange splitting of the bands, as already mentioned, since mainly the states of atoms, with spin up, contribute here. In general, more spin up states are thus occupied. A closer look on this peak is given through figure 6.7. The main contribution for this high density of states around zero energy is due to the atoms 2, 3, 5 and 7, which have all a net magnetization of spin up.

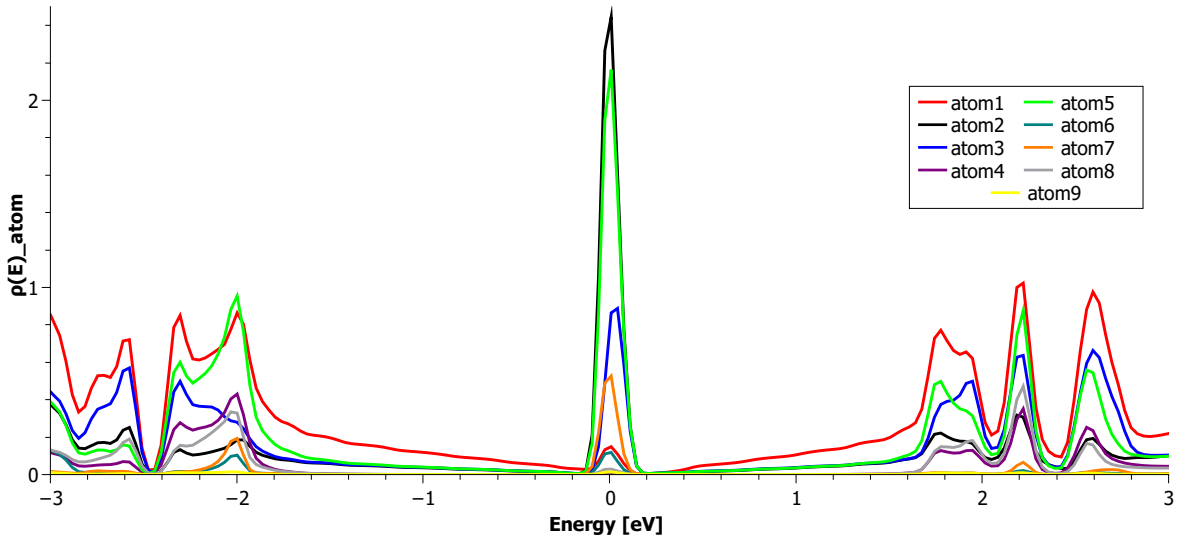

Figure 6.6: Atomic resolved DOS

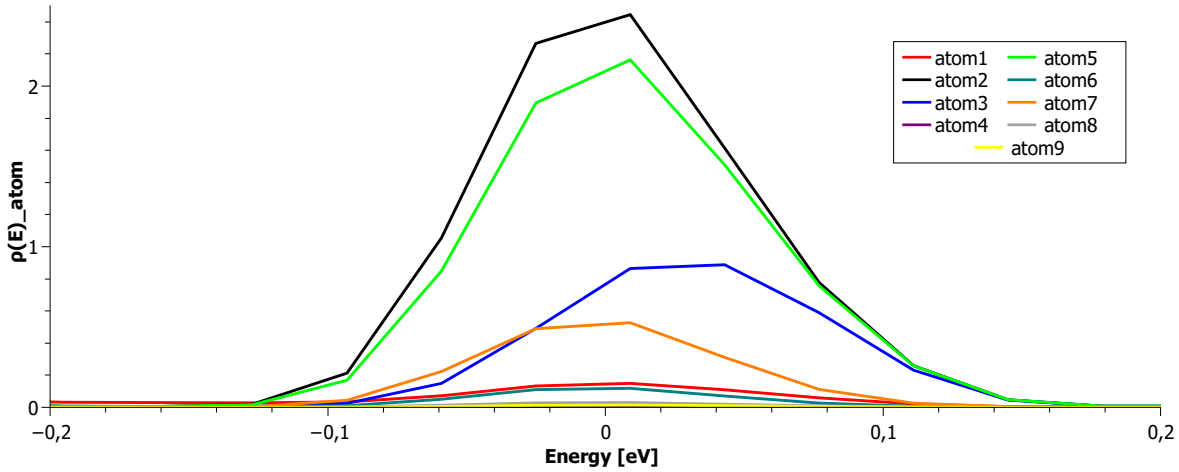

Figure 6.7: Peak around zero energy of atomic resolved DOS

Figure 6.8 shows the density of states for the net magnetization, meaning, that it shows the sum of the atomic densities of states, when taking their sign of the magnetic moment from table 6.2 into account

$$\begin{aligned}\rho(E)_{\text{magnetic}} &= \sum_{i=1}^{9} \pm\rho(E)_{\text{atom}i} \\ &= -\rho(E)_{\text{atom1}} + \rho(E)_{\text{atom2}} + \rho(E)_{\text{atom3}} - \rho(E)_{\text{atom4}} + \dots\end{aligned} \tag{6.2}$$

Only around zero energy, the states from spin up and spin down do not compensate each other, since there are more spin up states, than spin down states occupied.

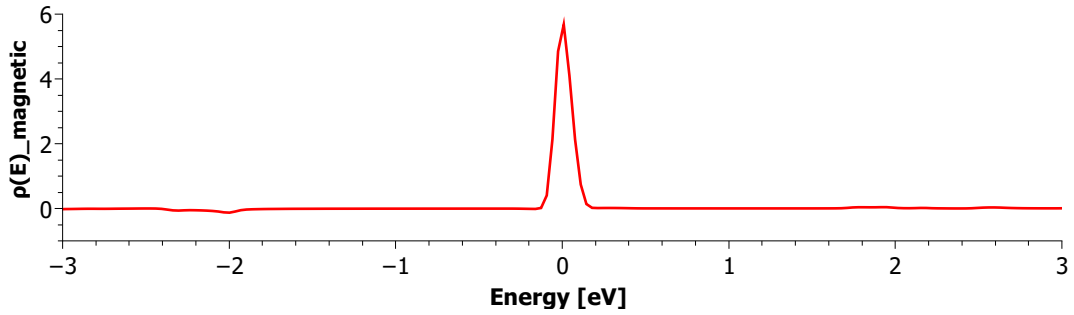

Figure 6.8: Density of states for net magnetization. Spin up and down compensate each other, but not around zero energy

A closer look on the orbital resolved DOS, for the atoms, which are involved in the bonding to the methyl group (namely atoms 5, 6, 7 and 9), is shown in figure 6.9. As one can see, the main contribution of the hydrogen atoms (atom 9) is due to the s orbitals. The contribution from atom 5 is mainly due to p_z orbitals.
As one can expect, the main contributions from atoms 6 and 7 should be due to p_z states, since the bonding is perpendicular to the graphene layer, which is in fact the case. The density of states thus directly contains information about the direction of the bonding. Note, that atom 7 has a not negligible contribution from s states. Again, the orbital contributions do not reach the total DOS value, as before.

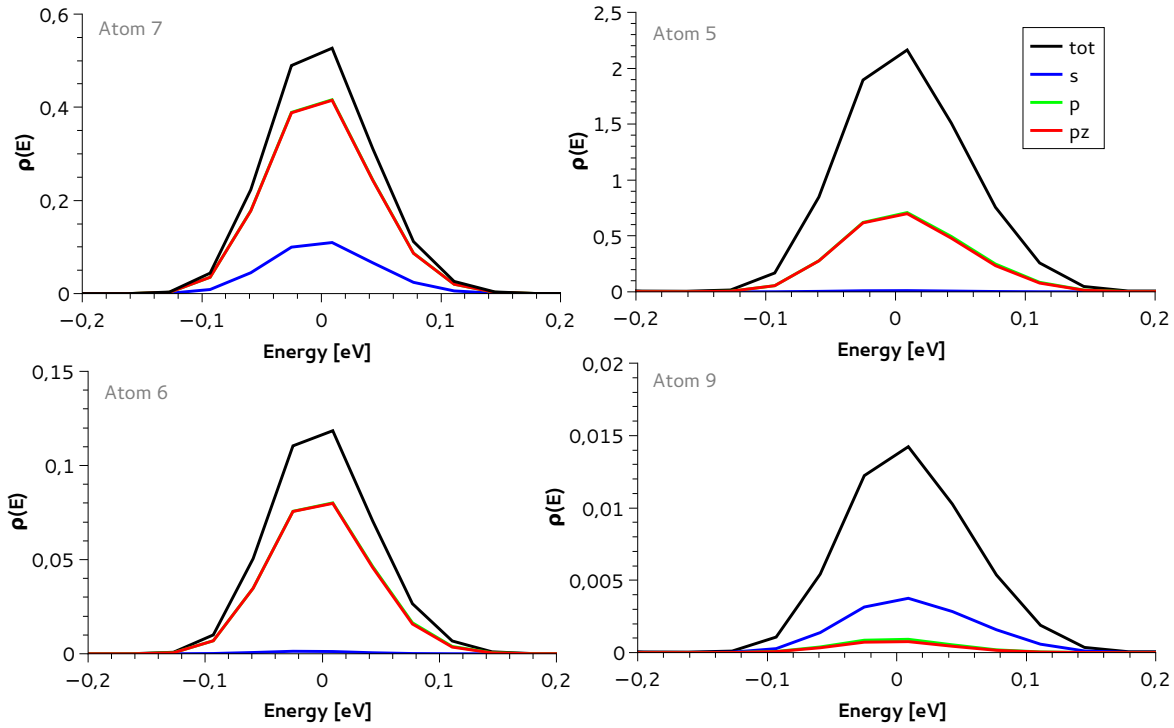

Figure 6.9: Orbital resolved DOS at zero energy peak for atoms located around methyl group

The spin resolved DOS is shown in figure 6.10 for $RK = 4$ and a k-point sampling of $15 \times 15 \times 1$. One can definitely confirm the fact of the antisymmetric filling of spin up and spin down states, leading to a net magnetic moment.

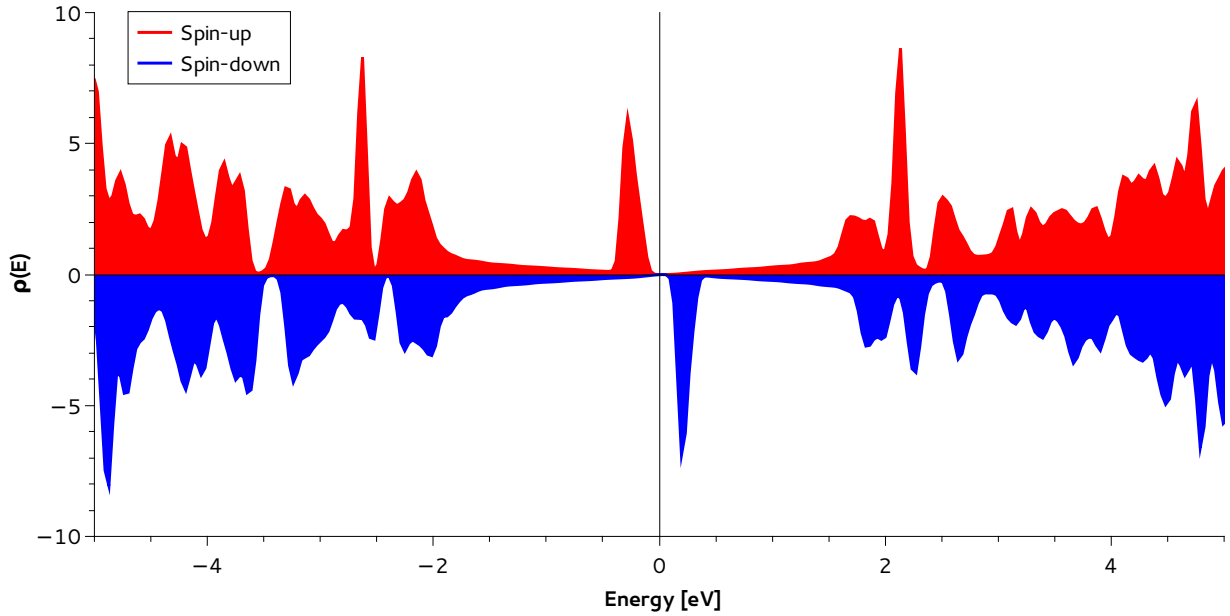

Figure 6.10: Spin resolved DOS of methylated graphene

7 Overview and Outlook

In the thesis we studied the electronic structure of graphene and methylated graphene with ab-initio calculations. Starting from considering pure single layer graphene sheets, we investigate graphene where methyl groups were attached.

During the study of graphene structures, with Wien2k, a lot of practical knowledge, concerning ab-initio codes and DFT, has been gained. The main problem in condensed matter physics was stated, solution approaches were made and fundamentals of DFT were introduced. We considered the theorems of Hohenberg and Kohn, which are the foundations of DFT, that led to the self-consistent Kohn-Sham equations, which are a practical tool, in order to determine the ground state of a solid. Different basis sets were introduced, which are crucial, when calculating electronic properties, since the electronic density is obtained by the square of the absolute value of the wave function. One gained expertise in handling the Wien2k software suite and knowledge about post-processing, like calculating the density of states or band structure. A feeling for crucial parameters and convergence quantities evolved.

The first results we obtained were the band structure and the density of states, by considering pure single layer graphene. These quantities were in quite good agreement with the thight-binding ones, since we could confirm the linear behavior of the DOS and the band structure at the neutrality points, which refers to massless Dirac fermions in the vicinity of the K-points, like they were theoretically predicted.

The more interesting part, where we considered methylated graphene, led to a spin splitting and thus an antisymmetric filling of the states, resulting in a net magnetic moment of 1 μ_B per unit cell. We also found, that the DOS has a rather high value at the Fermi level, which indicates the exchange splitting. As expected, a gap in the band structure occured and the Dirac cone appeared now at the Γ-point, due to the fact, that the K-point of the Brillouin zone from the methylated graphene matches with the Γ-point of the graphene Brillouin zone.

Due to the lack of time, it was not possible to obtain the ideal results for the methylated graphene, as this would need more calculations with different unit cell constants. One could have also treated spin-orbit coupling or other quantities, concerning different unit cells, where the number and orientation of the methyl groups varies, as one can in principle expect a change in the value of the total magnetic moment or a change in the size of the band splitting. In particular, it would be interesting, what happens if other adatoms or

admolecules (such as Fluorine or Hydrogen) were attached and not a methyl group. And it would also be possible to use different two dimensional structures (single layer boron nitride) or additionaly consider vacancies in the structure. Moreover one could consider so called *Van-der-Waals heterostructures*, where several two dimensional structures are stacked on top of each other.

Appendix

A.1 Procedure and Parameters of WIEN2k

A.1.1 Single layer graphene

To reproduce the given results of the calculations with WIEN2k, here is a step-by-step guidance, to obtain them. Special properties of settings, parameters and naming conventions of the input files for WIEN2k can be looked up in [10].
In order to recreate the lattice structure of the considered system, one has to construct a *structure file* (see fig. A.1), which defines the unit cell and is used as general input for the procedure. One should be careful here, as the positioning of the single parameters in the **.struct* file is very sensitive, meaning that even one blank can decide, if the next steps run or not. In order to avoid this, one can look at the structure file at *$WIENROOT/SRC_templates*.

```
Graphene

H  LATTICE,NONEQUIV.ATOMS:  1                 191 P6/mmm
MODE OF CALC=RELA          unit=bohr
 4.647804      4.647804      28.0      90.0      90.0      120.0

ATOM   1:       X=0.33333333  Y=0.66666667  Z=0.00000000
       MULT= 2          ISPLIT= 4
          1:       X=0.66666667  Y=0.33333333  Z=0.00000000
C 1       NPT=  781       R0=0.0001       RMT=   1.33      Z:  6.0

 24     NUMBER OF SYMMETRY OPERATIONS
```

Figure A.1: Structure file of graphene

In the *initalization* process of the *LAPW* routine [`init_lapw`], one uses the new scheme with a reduction of RK of 0%. As the *muffin tin radius* RMT is already set in the structure file, one can use these values and take a *next neighbour bond-length* factor of 2. Spin of the electrons is not important in this calculation, so it can be set to (default). The configuration for *lstart* is the PBE-GGA and a *separation energy* (between core and valence states) of -6 Ry has been chosen. The k-point sampling in *kgen* can be arbitrarily set to $5 \times 5 \times 1$ for a first calculation.
For the actual calculation, one has to run *LAPW*, with the *charge convergence* option

[`run_lapw -cc 0.0001`], which means, that if a charge convergence less than 10^{-4} is obtained,

$$\Delta c = \int |\rho_n(\boldsymbol{r}) - \rho_{n-1}(\boldsymbol{r})| dr < 10^{-4} \cdot e \tag{A.1}$$

the routine can stop, because the result is acceptable. A closer look on the whole routine, can be found in Ref. [10] or look at figure A.6. One can look into the **.scf* file to get the energies ENE [`grep :ENE *.scf`] and FER and the number of basis functions RKM from the **.scf1* file. A calculation with a force relaxation is not necessary, since one exactly knows how the honeycomb structure of graphene looks like with all the distances and angles. But this will be important later. In principle one should also do a determination of the lattice constant.
After several calculations with different RK = $R_\alpha^{min} K_{max}$ and different k-point samplings (KPTS) (see A.1) one finds the optimal parameter for graphene from the figures A.3, A.4 and A.5. One can see, that the total energy (ENE) converges for RK=8 and KPTS=40 and has its minimal value ($\Delta(\text{ENE})_{RK=\{7,8\}} \approx 14$ meV, $\Delta(\text{ENE})_{RK=\{8,9\}} \approx 7$ meV). Figure A.5 shows, that the Fermi energy (FER), obtained from the calculation, is only accurate when KPTS is dividable by 3 (maybe only these k-point samplings are good, when at the Dirac cone (see figure A.2). Pretend, that one sampling takes the points 1-3 and another one just takes the points 2 and 3. Then the Fermi energy, which is for graphene at the dirac point, would be shifted by a ΔE) and therefore we use KPTS to be 48, which equals a k-sampling of $21 \times 21 \times 1$.

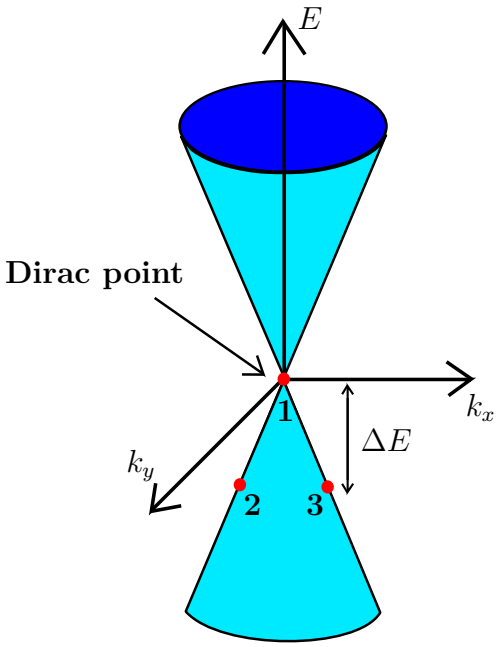

Figure A.2: Sketch of the dirac cone and the sampling points/KPTS (red)

One also obtains, that one has to set G_Max =14 to satisfy G_Min < G_Max. As the spin is not important, we do not need a spin polarized calculation.

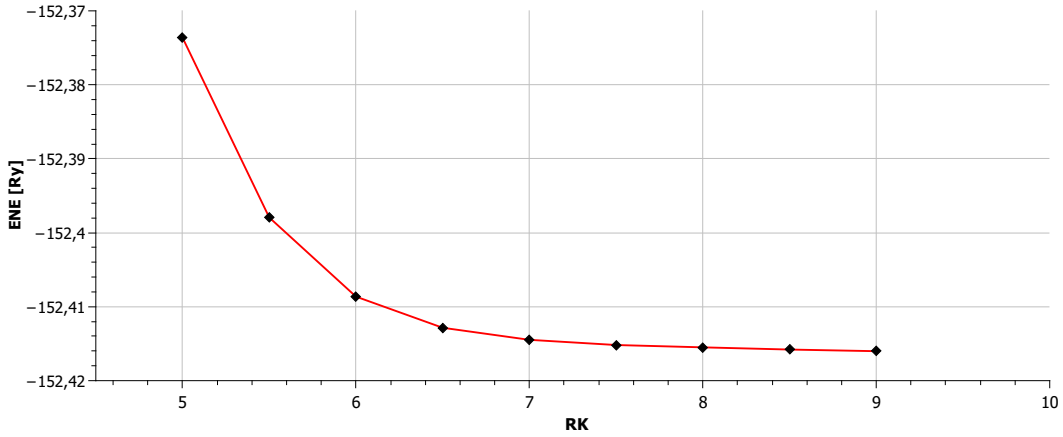

Figure A.3: Total energy (ENE) as a function of $R_{\alpha}^{min} \cdot K_{max}$ (RK)

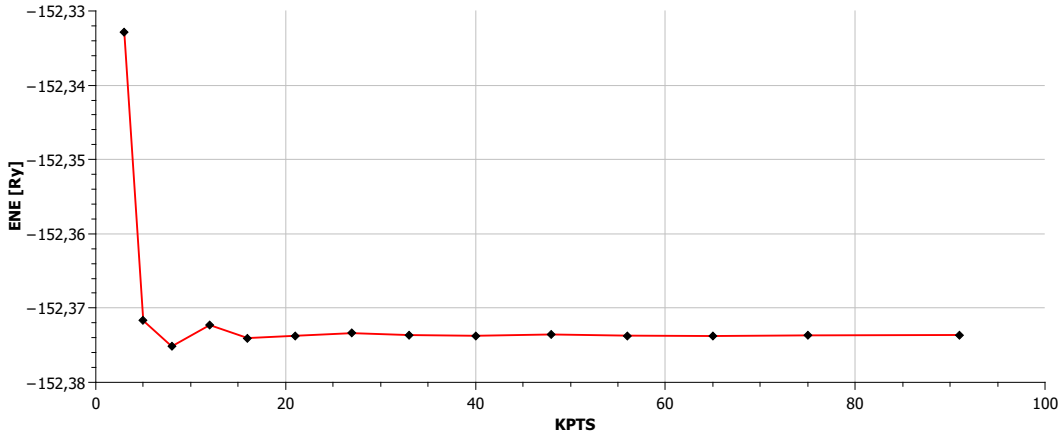

Figure A.4: Total energy (ENE) as a function of k-points (KPTS)

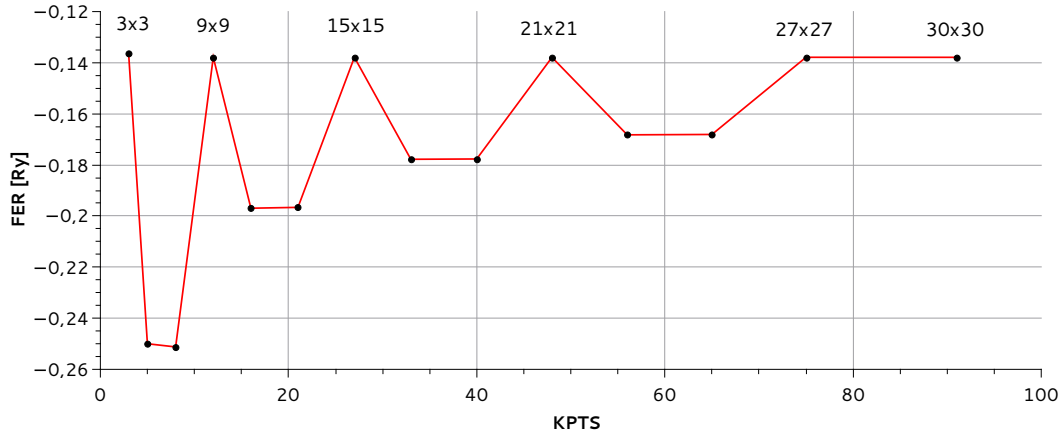

Figure A.5: Fermi energy (FER) as a function of k-points (KPTS)

To construct the band structure (see figure 5.2) one first has to define the path in the k-space (here: $\Gamma - M - K - \Gamma$ was chosen), along which the band structure has to be calculated. This can be easily done with Xcrysden [`xcrysden -wien_kpath *.scf`] when separating this path into 100 k-points. Next, one needs an **.insp* file, which can be copied from *$WIENROOT/SRC_templates* directory and in this file the Fermi energy from the **.scf* file has to be inserted. Now one has to execute *lapw1* [`x lapw1 -band`], *lapw2* [`x lapw2 -band -qtl`] and *spaghetti* [`x spaghetti -qtl`]. *lapw1* calculates the eigenvalues along the defined path and *lapw2* calculates the particle charges. To visualize the band structure, one can for example look at the **.spaghetti_ps* file, or directly plot the energies from the **.spaghetti_ene file*.
To construct the density of states (DOS) one first has to change the k-point sampling to $42 \times 42 \times 1$ and rerun the *lapw* calculation, in order to get a better accuracy, when calculating the DOS. To calculate the particle charges one has to execute *lapw2* [`x lapw2 -qtl`]. To run the program *tetra* one needs the input file **.int*, which allows to specify which partial DOS should be calculated. To create this file we run [`configure_int_lapw`] and take the DOS up to d-charakter. Now one can run the program *tetra* [`x tetra -qtl`], which creates the files for the DOS, namely **.dos1* and **.dos1ev*.

RK	KPTS	K-Matrix	ENE	FER	G-MAX
5	3	3-3-1	-152.33284665	-0.1362372675	12
5	5	5-5-1	-152.37169405	-0.2499799629	12
5	8	7-7-1	-152.37515635	-0.2512280607	12
5	12	9-9-1	-152.37229051	-0.1378930738	12
5	16	11-11-1	-152.37403870	-0.1969413528	12
5	21	13-13-1	-152.37373221	-0.1966123952	12
5	27	15-15-1	-152.37337674	-0.1378933172	12
5	33	17-17-1	-152.37363437	-0.1777933982	12
5	40	19-19-1	-152.37373008	-0.1776751748	12
5	48	21-21-1	-152.37355481	-0.1379047334	12
5	56	23-23-1	-152.37371094	-0.1682302410	12
5	65	25-25-1	-152.37376299	-0.1680817486	12
5	75	27-27-1	-152.37367635	-0.1378826053	12
5	91	30-30-1	-152.37362400	-0.1378991160	12
5.5	27	15-15-1	-152.39794013	-0.1392064597	12
6	27	15-15-1	-152.40863779	-0.1375914936	12
6.5	27	15-15-1	-152.41284774	-0.1386237232	12
7	27	15-15-1	-152.41447826	-0.1382344157	12
7.5	27	15-15-1	-152.41518107	-0.1379355179	12
8	27	15-15-1	-152.41549579	-0.1376855797	12
8.5	27	15-15-1	-152.41579341	-0.1375221064	12
9	27	15-15-1	-152.41601528	-0.1374234363	12
9	27	15-15-1	-152.41534335	-0.1374047123	14
8.5	27	15-15-1	-152.41527412	-0.1375035393	14
8	27	15-15-1	-152.41512965	-0.1376957228	14
7.5	27	15-15-1	-152.41480993	-0.1379314856	14
7	27	15-15-1	-152.41412098	-0.1382317673	14
6.5	27	15-15-1	-152.41250934	-0.1386189860	14
6	27	15-15-1	-152.40832866	-0.1375791639	14
5.5	27	15-15-1	-152.39767181	-0.1392024130	14
5	27	15-15-1	-152.37314794	-0.1378956351	14

Table A.1: Set of calculations to obtain ideal parameters

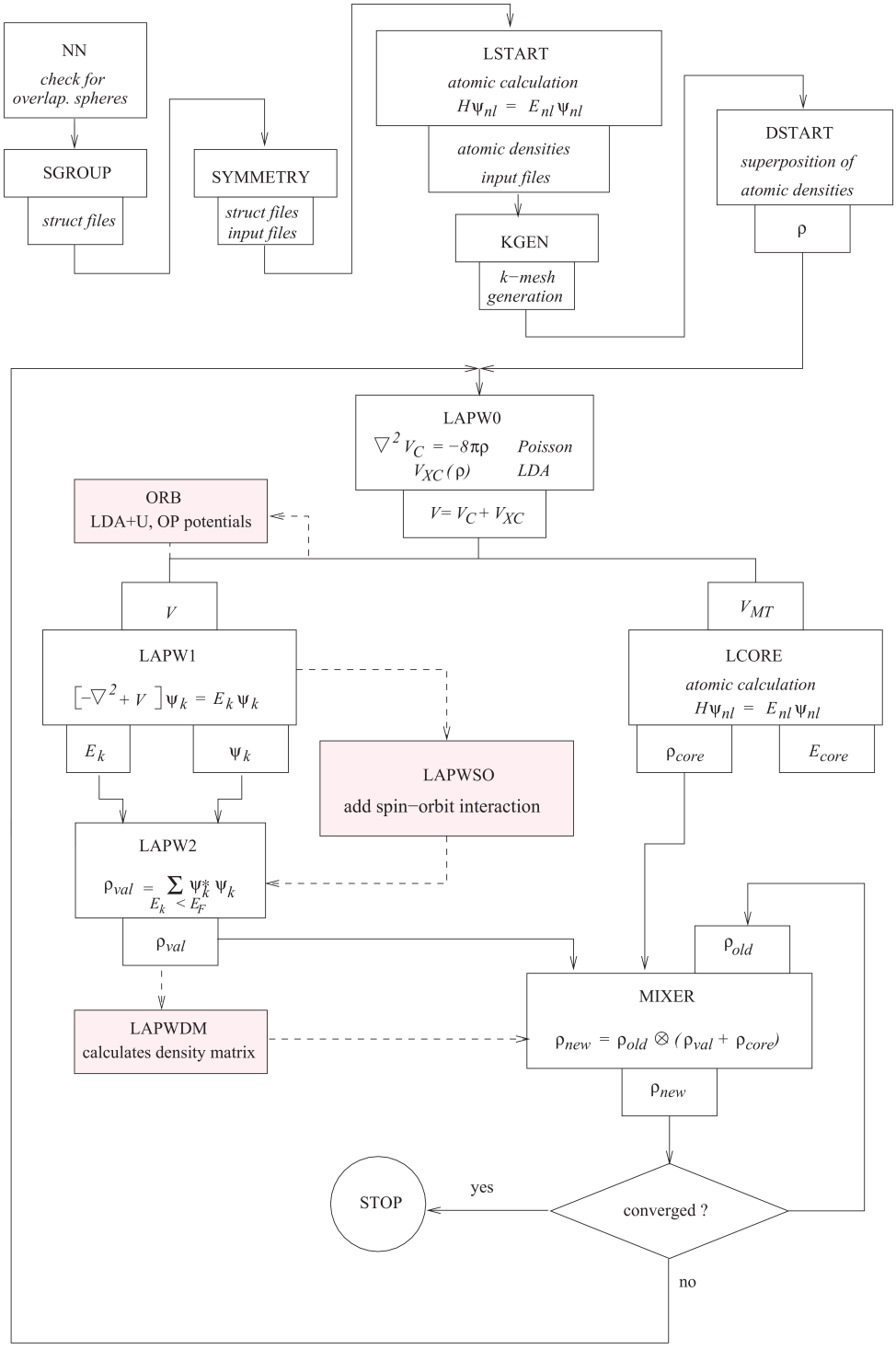

Figure A.6: Program flow in WIEN2k [10]

A.1.2 Methylated graphene structure

The calculations for the graphene structure with the methyl group attached were more difficult to perform. One has to create a *supercell* [`x supercell`], because one cannot attach a methyl group to every carbon atom, as they would overlap and we only want to consider them as a kind of impurity. The unit cells for the two different modifications are shown in figure 6.1, and contain a lot more than only two carbon atoms. The final *structure* files are shown in (A.7, A.8), but the mentioned unit cells do not match with these structure files. This is because, when *initializing LAPW*, the structure files are changed in the symmetry cycle.
The rest of the initialization is equal to the one of graphene except, that the parameter $RK = R_{\alpha}^{min} K_{max}$ was chosen to be between 3.5 and 4.5 and *'de' (emax = Ef + de)* to be 0.5 in the **.in1c* file. The k-point sampling was chosen to be $5 \times 5 \times 1$ and ran with the options [`run_lapw -cc 0.001 -p`]. The option *-p*, means, that the calculation runs parallel on different cores of the processor. For that, one has to create a *.machines* file, where the number of parallel calculations is declared, for parallelizing k-points over processors.
As this calculation lead to no error, the next step was to optimize the structure, by executing a force relaxation. Therefore one needs to edit the **.inm* file and use *MSR1a* as mixing method. Now one runs again the LAPW cycle [`run_lapw -cc 0.0001 -fc 1 -p`] with the additional force convergence parameter. This leads to a slightly modified structure, where the mentioned tetrahedral shape is much more pronounced. The forces from the **.scf* [`grep :FR *.scf`] should reduce themselves to an acceptable value (in general at the order of *mRyd/bohr*). The force relaxation has to be performed for structures, where one just approximately knows the geometry of the system, but it is important to find the configuration of the atoms, where the energy is minimal, as it depends on the positions of the nuclei.
As already mentioned, one can in principle expect a magnetic moment in this structure, due to the covalently bonded methyl group. Therefore one considers a calculation with spin-polarization, different RK and k-point samplings [`runsp_lapw -cc 0.0001 -p`]. The band structure and the DOS are obtained by an analogue procedure as for graphene, with the difference, that one has to add the option [`-up|dn`] either for spin up or spin down calculation.

```
Graphene_Supercell_1

H                    9                                  156 P3m1
         RELA
 13.943412      13.943412       28.0      90.0     90.0     120.0

ATOM  -1:       X=0.33341822  Y=0.00103979  Z=0.99044940
       MULT= 6        ISPLIT= 8
    -1:  X=0.99896021  Y=0.33237843  Z=0.99044940
    -1:  X=0.66762157  Y=0.66658178  Z=0.99044940
    -1:  X=0.99896021  Y=0.66658178  Z=0.99044940
    -1:  X=0.66762157  Y=0.00103979  Z=0.99044940
    -1:  X=0.33341822  Y=0.33237843  Z=0.99044940
C 1      NPT=  781       R0=0.0001      RMT=    1.2800          Z:   6.0

ATOM  -2:       X=0.44438258  Y=0.88876516  Z=0.99255572
       MULT= 3        ISPLIT= 8
    -2:  X=0.11123484  Y=0.55561742  Z=0.99255572
    -2:  X=0.44438258  Y=0.55561742  Z=0.99255572
C 2      NPT=  781       R0=0.0001      RMT=    1.2800          Z:   6.0

ATOM  -3:       X=0.77812424  Y=0.88906212  Z=0.98590836
       MULT= 3        ISPLIT= 8
    -3:  X=0.11093788  Y=0.88906212   Z=0.98590836
    -3:  X=0.11093788  Y=0.22187576  Z=0.98590836
C 3      NPT=  781       R0=0.0001      RMT=    1.2800          Z:   6.0

ATOM  -4:       X=0.00000000  Y=0.00000000  Z=0.98505065
       MULT= 1        ISPLIT= 4
C 4      NPT=  781       R0=0.0001      RMT=    1.2800          Z:   6.0

ATOM  -5:       X=0.44094843  Y=0.22047421  Z=0.99676014
       MULT= 3        ISPLIT= 8
    -5:  X=0.77952579  Y=0.22047421  Z=0.99676014
    -5:  X=0.77952579  Y=0.55905157  Z=0.99676014
C 5      NPT=  781       R0=0.0001      RMT=    1.2800          Z:   6.0

ATOM  -6:       X=0.66666667  Y=0.33333333  Z=0.02632690
       MULT= 1        ISPLIT= 4
C 6      NPT=  781       R0=0.0001      RMT=    1.2800          Z:   6.0

ATOM  -7:       X=0.66666667  Y=0.33333333  Z=0.13501101
       MULT= 1        ISPLIT= 4
C 7      NPT=  781       R0=0.0001      RMT=    1.2800          Z:   6.0

ATOM  -8:       X=0.33333333  Y=0.66666667  Z=0.99216132
       MULT= 1        ISPLIT= 4
C 8      NPT=  781       R0=0.0001      RMT=    1.2800          Z:   6.0

ATOM  -9:       X=0.74715961  Y=0.49431923  Z=0.16079821
       MULT= 3        ISPLIT= 8
    -9:  X=0.50568077  Y=0.25284039  Z=0.16079821
    -9:  X=0.74715961  Y=0.25284039  Z=0.16079821
H 1      NPT=  781       R0=0.0001      RMT=    0.7000          Z:   1.0

  6     NUMBER OF SYMMETRY OPERATIONS
```

Figure A.7: Structure file of methylated graphene; top configuration

```
Graphene_Supercell_2

H                    9                                    156 P3m1
         RELA
 13.943412      13.943412       28.0     90.0     90.0      120.0

ATOM  -1:       X=0.33332171  Y=0.00097206  Z=0.99104937
       MULT= 6        ISPLIT= 8
    -1:  X=0.99902794  Y=0.33234965  Z=0.99104937
    -1:  X=0.66765035  Y=0.66667829  Z=0.99104937
    -1:  X=0.99902794  Y=0.66667829  Z=0.99104937
    -1:  X=0.66765035  Y=0.00097206  Z=0.99104937
    -1:  X=0.33332171  Y=0.33234965  Z=0.99104937
C 1      NPT=  781      R0=0.0001      RMT=    1.2800          Z:   6.0

ATOM  -2:       X=0.44437043  Y=0.88874086  Z=0.99318235
       MULT= 3        ISPLIT= 8
    -2:  X=0.11125914  Y=0.55562957  Z=0.99318235
    -2:  X=0.44437043  Y=0.55562957  Z=0.99318235
C 2      NPT=  781      R0=0.0001      RMT=    1.2800          Z:   6.0

ATOM  -3:       X=0.77815494  Y=0.88907747  Z=0.98672616
       MULT= 3        ISPLIT= 8
    -3:  X=0.11092253  Y=0.88907747  Z=0.98672616
    -3:  X=0.11092253  Y=0.22184506  Z=0.98672616
C 3      NPT=  781       R0=0.0001      RMT=    1.2800          Z:   6.0

ATOM  -4: X=0.00000000 Y=0.00000000 Z=0.98601299
       MULT= 1        ISPLIT= 4
C 4      NPT=  781       R0=0.0001      RMT=    1.2800          Z:   6.0

ATOM  -5: X=0.44073689 Y=0.22036845 Z=0.99701995
       MULT= 3        ISPLIT= 8
    -5:  X=0.77963155 Y=0.22036845 Z=0.99701995
    -5:  X=0.77963155 Y=0.55926311 Z=0.99701995
C 5      NPT=  781      R0=0.0001      RMT=    1.2800           Z:   6.0

ATOM  -6: X=0.66666667 Y=0.33333333 Z=0.02578298
       MULT= 1        ISPLIT= 4
C 6      NPT=  781       R0=0.0001      RMT=    1.2800          Z:   6.0

ATOM  -7: X=0.66666667 Y=0.33333333 Z=0.13296926
       MULT= 1        ISPLIT= 4
C 7      NPT=  781      R0=0.0001       RMT=    1.2800          Z:   6.0

ATOM  -8: X=0.33333333 Y=0.66666667 Z=0.99298184
       MULT= 1        ISPLIT= 4
C 8      NPT=  781       R0=0.0001      RMT=    1.2800          Z:   6.0

ATOM  -9: X=0.58580018 Y=0.41419982 Z=0.15816162
       MULT= 3        ISPLIT= 8
    -9:  X=0.58580018  Y=0.17160035  Z=0.15816162
    -9:  X=0.82839965  Y=0.41419982  Z=0.15816162
H 1      NPT=  781       R0=0.0001      RMT=    0.7000          Z:   1.0

  6     NUMBER OF SYMMETRY OPERATIONS
```

Figure A.8: Structure file of methylated graphene; hollow configuration

List of Figures

List of Tables

Bibliography

[1] Richard M. Martin, *Electronic Structure - Basic Theory and Practical Methods*, 2008, ISBN 97-805215344-0-6, Cambridge University Press

[2] S. Cottenier, *Density Functional Theory and the family of (L)APW-methods: a step-by-step introduction* (Instituut voor Kern- en Stralingsfysica, K.U.Leuven, Belgium), 2002, ISBN 90-807215-1-4
(URL: http://www.wien2k.at/reg_user/textbooks)

[3] John P. Perdew, Kieron Burke, Matthias Ernzerhof, *Generalized Gradient Approximation Made Simple*, Phys. Rev. Lett. 77, 1996
(URL: http://journals.aps.org/prl/pdf/10.1103/PhysRevLett.77.3865)

[4] Klaus Capelle, *A Bird's-Eye View of Density-Functional Theory*
(URL: http://arxiv.org/abs/cond-mat/0211443v5)

[5] M. Born, R. Oppenheimer, *Zur Quantentheorie der Molekeln*, Annalen der Physik. 389, Nr. 20, 1927, S. 457–484
(URL: http://onlinelibrary.wiley.com/doi/10.1002/andp.19273892002/pdf)

[6] P. M. Chaikin, T. C. Lubensky, *Principles of condensed matter physics*, 1995, ISBN 0-521-43224-3, Cambridge University Press

[7] Efthimios Kaxiras, *Atomic and electronic structure of solids*, 2003, ISBN 978-0-521-81010-4, Cambridge University Press

[8] P. Hohenberg, W. Kohn, *Inhomogeneous Electron Gas*, 1964, Physical Review Vol. 136, Nr. 3B
(URL: http://journals.aps.org/pr/abstract/10.1103/PhysRev.136.B864)

[9] W. Kohn, L. J. Sham, *Self-Consistent Equations Including Exchange and Correlation Effects*, 1965, Physical Review Vol. 140, Nr 4A
(URL: http://journals.aps.org/pr/abstract/10.1103/PhysRev.140.A1133)

[10] User's Guide WIEN2k, *An Augmented Plane Wave Plus Local Orbitals Program for Calculating Crystal Properties*
(URL: http://www.wien2k.at/reg_user/textbooks/usersguide.pdf)

[11] W. Kohn, *Electronic Structure of Matter - Wave Functions and Density Functionals*, Nobel Lecture, 1999
(URL: http://www.nobelprize.org/nobel_prizes/chemistry/laureates/1998/kohn-lecture.pdf

[12] Parr, Robert G; Yang, Weitao, *Density-Functional Theory of Atoms and Molecules*, 1994, Oxford University Press, ISBN 978-0-19-509276-9.

[13] A.H. Castro Neto, *The electronic properties of graphene*, Reviews of Modern Physics, Volume 81, January-March 2009
(URL: http://journals.aps.org/rmp/abstract/10.1103/RevModPhys.81.109)

[14] Boukhvalov, Katsnelson, Lichtenstein, *Hydrogen on graphene: Electronic structure, total energy, structural distortions and magnetism from first-principles calculations*, Physical Review B77, 035427
(URL: http://journals.aps.org/prb/abstract/10.1103/PhysRevB.77.035427)

[15] Nature Materials (2014), *Scalable production of large quantities of defect-free few-layer graphene by shear exfoliation in liquids*
(URL: http://www.nature.com/nmat/journal/vaop/ncurrent/full/nmat3944.html)

[16] A. Geim, K. Novoselov, *The rise of graphene*, Nature Mat., Vol. 6, 2007
(URL: http://www.nature.com/nmat/journal/v6/n3/full/nmat1849.html)

[17] M. Gmitra, D. Kochan, J. Fabian, *Spin-orbit coupling in hydrogenated graphene*, Phys. Rev. Lett. 110, 2013
(URL: http://journals.aps.org/prl/pdf/10.1103/PhysRevLett.110.246602)

[18] W. Li, M. Zhao, Y. Xia, R. Zhang, Y. Mu, *Covalent-adsorption induced magnetism in graphene*, J. Mat. Chem. Vol. 19, 2009
(URL: http://pubs.rsc.org/en/content/articlepdf/2009/jm/b908949g)

[19] T. Wehling, M. Katsnelson, A. Lichtenstein, *Impurities on graphene: Midgap states and migration barriers*, Phys. Rev. B, Vol. 80, 2009
(URL: http://journals.aps.org/prb/pdf/10.1103/PhysRevB.80.085428)

[20] J. Zhou, Q. Liang, J. Dong, *Enhanced spin-orbit coupling in hydrogenated and fluorinated graphene*, Carbon, Vol. 48, 2010
(URL: http://www.sciencedirect.com/science/article/pii/S0008622309008434/pdfft?md5=9362fc16eb7d82cd1713ed410b8992dc&pid=1-s2.0-S0008622309008434-main.pdf)

[21] A.L. Allred, *Electronegativity values from thermochemical data*, Journal of Inorganic and Nuclear Chemistry, Vol. 17, 1961
(URL: http://www.sciencedirect.com/science/article/pii/0022190261801425#)

[22] E.H. Lieb, *Two Theorems on the Hubbbard Model*, Phys. Rev. Lett., Vol. 62, 1989
(URL: http://journals.aps.org/prl/pdf/10.1103/PhysRevLett.62.1201)

Erklärung gemäß § 32, Abs. (5) der Prüfungsordnung vom 29. November 2011

Ich erkläre hiermit, dass ich

- die vorliegende Abschlussarbeit selbstständig verfasst,
- keine anderen als die angegebenen Quellen und Hilfsmittel benutzt und
- die Arbeit nicht bereits an einer anderen Hochschule zur Erlangung eines akademischen Grades eingereicht habe.

Weiterhin bestätige ich hiermit, dass

- die vorgelegten Druckexemplare und die vorgelegte elektronische Version der Arbeit identisch sind,
- ich über wissenschaftlich korrektes Arbeiten und Zitieren aufgeklärt wurde und
- von den in § 24, Abs. (5) vorgesehenen Rechtsfolgen Kenntnis habe.

....

(Ort, Datum) (Unterschrift)